nature communications

Article

https://doi.org/10.1038/s41467-024-54757-2

Rab8a restores diverse innate functions in CD11c^{+}CD11b^{+} dendritic cells from aged mice

Received: 10 August 2023

Accepted: 17 November 2024

Published online: 27 November 2024

Check for updates

Sudhakar Singh, Azeez Tehseen, Surbhi Dahiya, Yuviana J. Singh, Roman Sarkar & Sharvan Sehrawat

Age-related alterations of the immune system compromise the host's ability to respond to pathogens, but how immune aging is regulated is still poorly understood. Here, we identify via transcriptomic analysis of splenic DCs and bone marrow derived dendritic cells (BMDC) of young and aged mice, the small GTPase Rab8a as a regulator of dendritic cell (DC) functions in mice. CD11c^{+}CD11b^{+} DCs of aged in comparison to young host exhibit a diminished type I IFN response upon viral stimulation and inefficiently present exogenous antigens to CD8^{+} T cells in vitro and in vivo. Rab8a overexpression, which is accompanied by the upregulation of Rab11, restores the functionality of these aged DCs, whereas knockdown of Rab8a reduces functionality of DCs from young mice. Mechanistically, Rab8a and Rab11 cooperate to induce efficient trafficking of peptide loaded class I MHC molecules from the ER to the cell surface. We propose that targeting Rab8a might serve as a strategy to restore DC functionality in the context of immune aging.

Dendritic cells (DC) are the sentinel cells of the immune system owing to their strategic location at tissue sites and the abundant production of type I interferons (IFNs) early after virus infection. Accordingly, a compromised IFN response results in poor viral control. DCs link innate and adaptive immune responses and efficiently activate T cells[1]. Immune functions are lost progressively as the host ages. Consequently, the aging individuals become exceedingly susceptible to virus infections and develop severe disease when infected[2]. Several factors, which include the altered architecture and composition of microenvironment in lymphoid tissues, dysregulated migratory properties of immune cells, and an inefficient production of soluble mediators, can contribute to the compromised immunity in the aging host[3]. Reduced numbers of naive T and B cells as well as their slower turnover rates are evident in the aged population[4,5]. Innate immune cells of the aging host also exhibit impaired cytokine signalling, phagocytosis and antigen-uptake[6]. Therefore, the underlying complexity of immunosenescence makes its reversal challenging.

Morphological features, efficient antigen uptake and slower lysosomal proteolysis increase antigen dwell time to make DCs efficient antigen presenters[7,8]. Following antigen uptake, the processed peptides in context with MHC molecules are transported to the surface to induce T cell response[9,10]. The role of small GTPases like Rab8a in the surface transport of receptors and in maintaining cellular morphology has been extensively studied in cells other than DCs[11]. Furthermore, Rab11a has been shown to accumulate in the endosomal recycling compartment (ERC) with the loaded peptide-MHC molecules in response to TLR stimulation[12]. How Rab8a influences DC function has not been studied.

Here, we perform a genome-wide transcriptomic analysis of CD19^{-ve}CD3ε^{-ve}CD11c^{+ve}CD11b^{+ve} splenocytes and GM-CSF + IL-4 differentiated bone marrow derived dendritic cells (BMDCs) referred to as GM-CSF + IL4 CD11c^{+}CD11b^{+} cells of unmanipulated young and aged mice to identify molecular signatures associated with impaired immune functions. DCs of aged animals exhibit downregulation of multiple genes involved in differentiation, maturation and functionality. The expression of several IFN-stimulating genes (ISG) and of the small GTPase Rab8a is lower in the sorted CD11c^{+}CD11b^{+} cells of aged animals and humans compared with those of younger hosts. Reconstitution of Rab8a expression in aged DCs not only induces potent antiviral IFN activity but also enhances their ability to generate an efficient primary and memory response of anti-viral CD8^{+} T cells in influenza A virus (IAV) infected mice. We, therefore, show that Rab8a is critically

Department of Biological Sciences, Indian Institute of Science Education and Research Mohali, Sector 81, SAS Nagar Knowledge City PO Manauli, Mohali 140306 Punjab, India. e-mail: sharvan@iisermohali.ac.in

involved in the functioning of DCs of an aging host and its reconstitution might reinvigorate such cells to help achieve better outcome of infection in the context of aging.

Results and Discussion

Transcriptome analysis of DCs reveals compromised function in aging host

To gain insights into the molecular mechanisms responsible for the impaired functioning of DCs of an aging host, we performed a genome-wide RNAseq analysis of sorted $CD19^{-ve}CD3\varepsilon^{-ve}CD11c^{+ve}CD11b^{+ve}$ splenocytes of unmanipulated young (2 months) and aged (>24 months) mice (Supplementary Data 1, Fig. 1a and Supplementary Fig. 1a). For both the groups, the purity of sorted cells was over 95%. Out of 21519 genes, those showing an FPKM value of >5 in either sample were analysed for differential expression (Supplementary Fig. 1a). Comparative analysis showed that the splenic $CD19^{-ve}CD3\varepsilon^{-ve}CD11c^{+ve}CD11b^{+ve}$ cells upregulated 44 genes in young and 123 genes in the aged animals (Supplementary Fig. 1a). A large majority of such differentially expressed genes (DEGs) encode for the products which regulate signal transduction, several biological processes, cell-to-cell communication, and protein-protein or protein-nucleic acid interaction and hence were predominantly localised to cellular membrane or nucleus (Supplementary Fig. 1b–g). Genes upregulated in the cells of aged animals included those responsible for encoding inhibitory molecules as well as those associated with NK cells. Accordingly, the sorted cells of aged in comparison to young animals upregulated *Cd160* (5-fold), *Klrb1b* (3-fold), *Klrb1c* (4.5-fold), *Klrc1* (3.8 fold), *Klre1*(3.2-fold) and several GTPase-associated nucleotide-binding proteins such as *Gimap3* (4.15-fold), *Gimap4* (3.7-fold), *Gimap7* (3.6-fold), *Gimap5* (3.3-fold), *Gimap8* (3.2-fold), *Gimap6* (2.9-fold), *Gimap9* (2.3-fold), *Gimap1* (2.19-fold) (Fig. 1b, c)[13–16]. GIMAPs are critical for the survival of T cells but their role is yet to be evaluated in DCs' biology[17]. *Arl4d*, a GTPase, that negatively regulates the functioning of $CD8^+$ T cells, was upregulated by ~3.6-fold in the cells of aged in comparison to young mice[18]. Functional annotation, network, and pathway analysis of the significantly downregulated genes in the cells of aged animals revealed a compromised anti-viral response, remodelling of tissues, differentiation of T_h1, T_h2, and T_h17 cells, functioning of NK cells, homing of leucocytes and TCR as well as cytokine signalling (Supplementary Fig. 2a–c). Several interferon stimulating genes (ISG) such as *Ifitm1* (~2.4 fold), *Ifi27l2a* (2 fold), *Ifit3* (1.74 fold), *Ifit1* (1.7 fold), *Oas1a* (2.5 fold), *Oasl2* (2.27 fold) and *Oas2* (1.9-fold) were downregulated by the sorted cells of aged in comparison to their counterparts from young animals (Fig. 1d, Supplementary Fig. 2d). *Plscr1*, which encodes for a protein to control HCMV infection via IFN pathway, was downregulated by ~1.73-fold in the cells of aged as compared to those of young mice. Genes involved in PI3K/MtorC1 signalling axis such as *Rab8a*, *Akt1*, and *Rps6kb1* as well as those responsible for the homing of immune cells such as *Itgae* (1.5-fold), *Ccr7, and Nr1h3* (1.5-fold) were also downregulated by the cells of aged than those of young animals (Fig. 1a, d and e, Supplementary Fig. 2d)[19,20]. Therefore, the DCs of aged animals showed a transcriptional programme associated with impaired homoeostatic as well as anti-viral response. Since the splenic $CD19^{-ve}CD3e^{-ve}CD11c^{+ve}CD11b^{+ve}$ cells showed differential expression of molecules usually associated with other cell types such as NK cells, macrophages and granulocytes, we phenotypically characterised such cells of young and aged animals. Of the gated $CD3\varepsilon^{-ve}CD19^{-ve}CD11c^{+ve}CD11b^{+ve}$ cells, young as well as aged animals had ~50% Ly6G and Ly6C positive cells (Supplementary Fig. 3a). Furthermore, ~5% $CD11c^+CD11b^+$ cells of young and ~10% of aged animals were NK1.1 positive. Therefore, splenic $CD19^{-ve}CD3\varepsilon^{-ve}CD11c^{+ve}CD11b^{+ve}$ splenocytes constituted a heterogeneous population and some of the observed DEGs could be due to the contaminating NK cells. Since DCs represent a small fraction of the total splenocytes, we therefore, used GM-CSF and IL-4 induced BMDCs (GM-CSF + IL-4 $CD11c^+CD11b^+$ cells) as a surrogate cell type to study the role of age-associated alterations. While the GM-CSF + IL-4 $CD11c^+CD11b^+$ cells of aged and young animals had similar proportions of contaminating $F4/80^+$, or $Gr1^+$ cells, the $NK1.1^+$ cells were significantly more in aged animals (Supplementary Fig. 3b).

Next, we measured the IFN response of the GM-CSF + IL-4 $CD11c^+CD11b^+$ cells of aged and young animals at basal levels as well as following stimulation with two different viruses, an Influenza A virus (WSN-SIINFEKL) and a γ-herpesvirus (MHV68-SIINFEKL) (Fig. 1f–j, Supplementary Fig. 4a–e). IAV pulsed cells of aged animals in comparison to those from their younger counterparts showed 15, 12 and 2-fold reduced levels of *Ifna, Ifnb* and *Ifng*, respectively (Fig. 1g). Similar results were obtained for the MHV68-stimulated GM-CSF + IL-4 $CD11c^+CD11b^+$ cells (Supplementary Fig. 4b). The JAK/STAT pathway predominantly transduces signal via IFN receptor (IFNR). Therefore, we measured the expression level of different downstream molecules in the pathway[21]. The expression of transcription factors; *Stat1, Stat2* and *Irf9* was significantly downregulated in the IAV or MHV68 stimulated GM-CSF + IL-4 $CD11c^+CD11b^+$ cells of aged in comparison to those of young animals (Fig. 1h, Supplementary Fig. 4c). Compared with the GM-CSF + IL-4 $CD11c^+CD11b^+$ cells of young animals, the cells of aged animals also had reduced expression of *Oas1a* (80 and 140-fold), *Oas1g* (8 and 4-fold), *Oas2* (5 and 4-fold), *Oas3* (9 and 4-fold), *Ifit1* (3 and 3-fold), *Ifitm1* (6 and 2-fold) and *Isg15 (6.4 and 4-fold)* following stimulation with IAV or MHV68, respectively (Fig. 1i, j, Supplementary Fig. 4d, e). Multiple cell surface (*Tlr1, Tlr2*, and *Tlr4*) and endosomal (*Tlr7, Tlr8*, and *Tlr9*) toll-like receptors (TLRs) as well as their downstream molecules such as *Myd88*, *Traf6*, *Irf7* and *Nfkb1* were significantly downregulated in the IAV stimulated GM-CSF + IL-4 $CD11c^+CD11b^+$ cells of aged when compared with those of young animals (Supplementary Fig. 5a–c). The production of pro- (*Il6* and *Il1b*) and anti- (*Il4* and *Il10*) inflammatory cytokines was also reduced by the IAV stimulated cells of aged in comparison to their counterparts of young animals (Supplementary Fig. 5d, e).

We then assessed whether a compromised IFN response is also observed in the IAV stimulated innate immune cells of aged compared to the young humans. Peripheral blood mononuclear cells (PBMCs) or the $CD11c^+CD11b^+$ enriched PBMCs of apparently healthy young (< 25 years) and aged (> 65 years) individuals were stimulated in vitro with IAV (Supplementary Fig. 6a). Compared to the cells of young humans, PBMCs as well as the $CD11c^+CD11b^+$ enriched PBMCs of aged humans showed reduced expression levels of most of the genes of IFN pathways (Fig. 1k–n, Supplementary Fig. 6b-e). Therefore, $CD11c^+CD11b^+$ cells of an aged host showed generic defects in IFN response.

DCs of an aging host induce compromised virus-specific $CD8^+$ T cell response

In addition to the direct anti-viral activities of IFNs, signalling via IFNR in antigen-presenting cells (APC) enhances the expression of MHC and costimulatory molecules for efficient induction of T cell response[22–24]. A compromised IFN response can increase the susceptibility of aged individuals to develop severe disease following infection with respiratory viruses such as SARS-CoV2 and IAV[25–30]. We, therefore, phenotypically characterised splenic $CD11c^+CD11b^+$ cells of aged, young, and IFN receptor knockout ($ifnr^{del}$) mice. Frequencies of $CD11c^+CD11b^+$ cells in aged, young, and $ifnr^{del}$ mice were 6.62% ± 0.2, 1.14% ± 0.2, and 1.91% ± 0.47, respectively (Supplementary Fig. 7a, b). $CD11c^+CD11b^+$ cells that expressed class I MHC molecules were also significantly less frequent in the aged (69.16 % ± 1.2) and $ifnr^{del}$ mice (59.9% ± 1.4) in comparison to those in young wild type (WT) animals (79.9% ± 2.17) (Supplementary Fig. 7c, d). Furthermore, the frequencies of $CD11c^+CD11b^+$ cells that expressed costimulatory molecules, CD80 and CD86, were significantly lesser in the aged (35.43% ± 1.5) as compared to young (49.03% ± 7.3) animals (Supplementary Fig. 7e, f).

https://doi.org/10.1038/s41467-024-54757-2

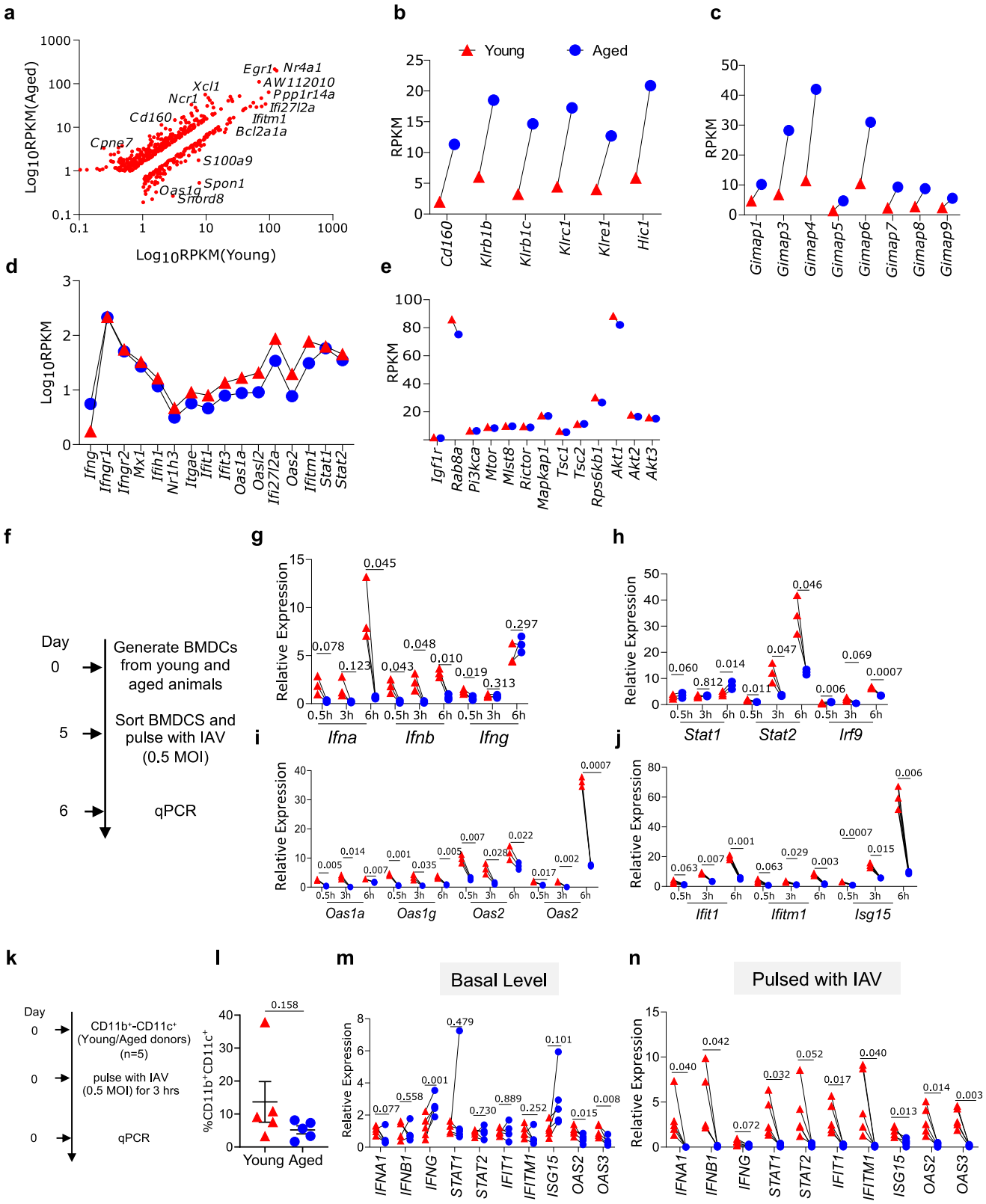

GM-CSF + IL-4 CD11c$^+$CD11b$^+$ cells from young, aged and ifnr^{del} mice were also similarly analysed. The cells that co-expressed CD80 and CD86 were significantly lesser in the aged (17.3% ± 0.36) and ifnr^{del} (27.2% ± 0.15) than those in the WT young (35.0% ± 1.2) mice (Fig. 2a, Supplementary Fig. 7g, h and j). Class I MHC expressing GM-CSF + IL-4 CD11c$^+$CD11b$^+$ cells in the aged and young mice were 70.60% ± 1.68 and 84.60% ± 0.17, respectively (Fig. 2a, Supplementary Fig. 7i, j). MHC class I and II expressing CD11c$^+$CD11b$^+$ cells were upto two-fold lesser in the age-matched ifnr^{del} (class I MHC^{+ve} cells 42.0% ± 1.04, class II MHC^{+ve} cells 56.07% ± 0.15) than those in the WT mice (Supplementary Fig. 7i).

While the CD8α$^+$CD11c$^+$ DCs are known to efficiently cross-present antigens, CD11c$^+$CD11b$^+$ conventional DCs can do so to activate CD8$^+$ T cells. Antigen cross-presentation is particularly relevant during vaccination and the resolution of infection with some

https://doi.org/10.1038/s41467-024-54757-2

Fig. 1 | Transcriptome analysis of CD3ε^{-ve}CD19^{-ve}CD11c^{+ve}CD11b^{+ve} splenocytes of young and aged animals reveal a compromised type I IFN response in the aged cells. a Dot plot shows the expression of genes in CD3ε^{-ve}CD19^{-ve}CD11c^{+ve} CD11b^{+ve} splenocytes of aged and young animals. **b** Graph shows the expression of key inhibitory genes differentially expressed by aged and young CD3ε^{-ve}CD19^{-ve}CD11c^{+ve}CD11b^{+ve} splenocytes. **c** Graphs show the expression GIMAP family genes in the splenic CD3ε^{-ve}CD19^{-ve}CD11c^{+ve}CD11b^{+ve} cells of aged and young mice. **d** Line graphs show log_{10} RPKM values for the expressed genes of type I IFN pathway in the splenic CD3ε^{-ve}CD19^{-ve}CD11c^{+ve}CD11b^{+ve} cells of young and aged animals. **e** RPKM values for the indicated genes responsible for differentiation of DCs in splenic CD3ε^{-ve}CD19^{-ve}CD11c^{+ve}CD11b^{+ve} cells of aged and young animals are shown. **f**–**j** Measuring the expression of IFNs and interferon stimulated genes (ISGs) in IAV stimulated GM-CSF + IL-4 CD11^{+}CD11b^{+} BMDCs of young and aged mice. **f** A schematic of the experiments is shown. The FACS-sorted GM-CSF + IL-4 CD11^{+}CD11b^{+} cells from young and aged mice were stimulated with 0.5 multiplicity of infection (MOI) of IAV (WSN-SIINFEKL) for the indicated time. The stimulated cells were processed for RNA isolation and cDNA synthesis. The relative expression of different genes of IFN pathway was then measured by quantitative reverse transcriptase (qRT)-PCR. **g**–**j** The relative expression of different genes involved in type I IFN pathway are shown. Three technical replicates were used for each group. The levels of statistical significance were analysed by a paired two-tailed t-test and the p-values are shown. **k**–**n** Measuring the expression of IFNs and ISGs in virus stimulated CD11c^{+}CD11b^{+} enriched PBMCs of young and aged humans. **k** Schematic for the experiment is shown. The PBMCs isolated from aged (> 65 years) and young (< 25 years) individuals were FACS sorted for CD11c^{+}CD11b^{+} cells (50×10^3) which were then stimulated with 0.5MOI of IAV for the indicated time points. The expression of different genes was analysed by qRT-PCR. **l** A plot summarising the frequency of the CD11b^{+}CD11c^{+} cells in each group is shown. Mean ± SEM values are indicated. Five biological replicates were used for each group. **m**, **n** Plots show the relative expression of the indicated genes of type I IFN pathways. Mean ± SEM values are shown. Five biological replicates were used for each group. The data is representative of three experiments. The levels of statistical significance were analysed by a paired two-tailed t-test and the p-values have been reported.

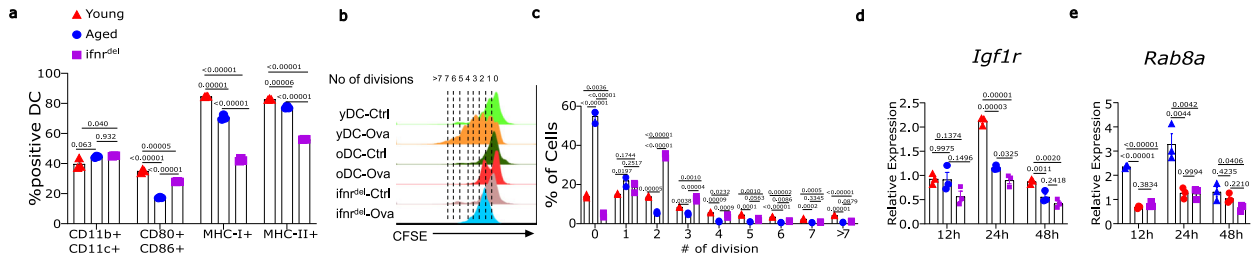

Fig. 2 | Phenotypic analysis of GM-CSF + IL-4 CD11c^{+}CD11b^{+} Bone Marrow Dendritic Cells (BMDC) of young, aged and interferon receptor knockout (ifnr^{del}) mice. Bone marrow from young, aged and ifnr^{del} mice were cultured in the presence of GM-CSF and IL-4 for 6 days for generating BMDC. The cells were then phenotypically characterized. **a** Bar graphs summarise the frequency of cells expressing the indicated markers. Three biological replicates were used for each conditions. The experiments were performed three time and the data from one of the representative experiments is shown. The levels of statistical significance were analysed by One-way ANOVA followed by Tukey Kramer post hoc test and the p-values are shown. **b**, **c** GM-CSF + IL-4 CD11c^{+}CD11b^{+} cells were FACS-sorted and pulsed with Ova for 2 hours. The washed cells were then co-cultured with CFSE labelled OT1 cells for 72 hours. CFSE dilution was then used as a measure of cell division. **b** Representative offset histograms show the frequency of proliferating CD8^{+} T cells in the indicated conditions. **c** Bar diagram shows data from one of the representative experiments. Three technical replicates were used for each condition. The levels of statistical significance were analysed by One-way ANOVA followed by Tukey Kramer post hoc test and the p-values are shown. The experiments were repeated more than five times and Mean ± SEM values are shown. **d**, **e** Bar graph shows relative expression of *Igf1r* (**d**) and *Rab8a* (**e**) in the FACS-sorted GM-CSF + IL-4 CD11c^{+}CD11b^{+} BMDCs at the indicated time points using qRT-PCR. For each group three technical replicates were used. The experiments were repeated three times and Mean ± SEM values are shown. The levels of statistical significance were analysed by One-way ANOVA followed by Tukey Kramer post hoc test and the P-values have been reported.

viruses[31–33]. To assess the antigen cross-presentation by FACS-sorted GM-CSF + IL-4 CD11c^{+}CD11b^{+} cells of aged, young and ifnr^{del} mice, we performed two types of experiments (Supplementary Fig. 8a). First, the soluble ovalbumin (Ova) pulsed BMDCs were co-cultured with CFSE labelled OT1 cells (K^{b}-SIINFEKL restricted TCR transgenic CD8^{+} T cells) in vitro. Compared to those of young mice, GM-CSF + IL-4 CD11c^{+}CD11b^{+} cells of aged mice induced significantly reduced expansion of OT1 cells (Fig. 2b, c). The cells of ifnr^{del} in comparison to those of WT mice also induced significantly reduced expansion of OT1 cells (Fig. 2b, c). To assess whether a delayed kinetics of antigen-uptake and subsequent processing contribute to the differential expansion of CD8^{+} T cells, GM-CSF + IL-4 CD11c^{+}CD11b^{+} cells of young, aged, and ifnr^{del} animals were pulsed with Ova for 2 and 24hrs. A prolonged incubation of these cells from young, aged and ifnr^{del} animals with Ova did not alter the response pattern (Supplementary Fig. 8b, c). Furthermore, the differentiated GM-CSF + IL-4 CD11c^{+}CD11b^{+} cells of young but not those of the aged or ifnr^{del} animals upregulated *Igf1r* and *Rab8a* which indicated a diminished cytokine sensing in the cells of aged and IFNR^{del} animals (Fig. 2d, e). The data show that the aged DCs as well as those lacking in IFN signalling are compromised in their innate immune functions.

We then evaluated in vivo functionality of GM-CSF + IL-4 CD11c^{+}CD11b^{+} cells of young, aged, and ifnr^{del} mice using an adoptive transfer approach. 5×10^5 of antigen-pulsed cells from young, aged and ifnr^{del} mice were injected in young CD45.1^{+} congenic animals that had received 6×10^4 of CD45.2^{+} OT1 cells one day earlier (Fig. 3a). The recipients showed equal distribution of OT1 cells the following day (Supplementary Fig. 8d). Fifteen days later, we observed a two-fold increase in the frequencies of OT1 cells in the peripheral blood of animals receiving GM-CSF + IL-4 CD11c^{+}CD11b^{+} cells of young as compared to those receiving the aged cells (Fig. 3b, Supplementary Fig. 8e). The animals were then intranasally infected with IAV (WSN-SIINFEKL) to recall the persisting donor OT1 cells. The recipients of GM-CSF + IL-4 CD11c^{+}CD11b^{+} cells of aged and ifnr^{del} mice showed a sharp decline in body weight while those receiving the cells of young animals did so minimally (Fig. 3c). At 7 days post infection (dpi), the frequencies of OT1 cells in the peripheral blood were 5.20% ± 0.34, 0.21% ± 0.29 and 0.52% ± 0.10 in the recipients of Ova pulsed cells of young, aged, and ifnr^{del} mice, respectively (Fig. 3d, e, Supplementary 8f). At 8dpi, the expanded OT1 cells were >10, 5, and 7-fold more abundant in medLN, spleen, and lungs of animals receiving the cells of young as compared to those infused with the cells of aged or the ifnr^{del} animals (Fig. 3e, f). CXCR3^{+} OT1 cells were significantly less in the recipients of Ova pulsed GM-CSF + IL-4 CD11c^{+}CD11b^{+} cells of aged and ifnr^{del} in comparison to those receiving the cells from younger mice (Fig. 3g, Supplementary Fig. 8g). CXCR3 is expressed

https://doi.org/10.1038/s41467-024-54757-2

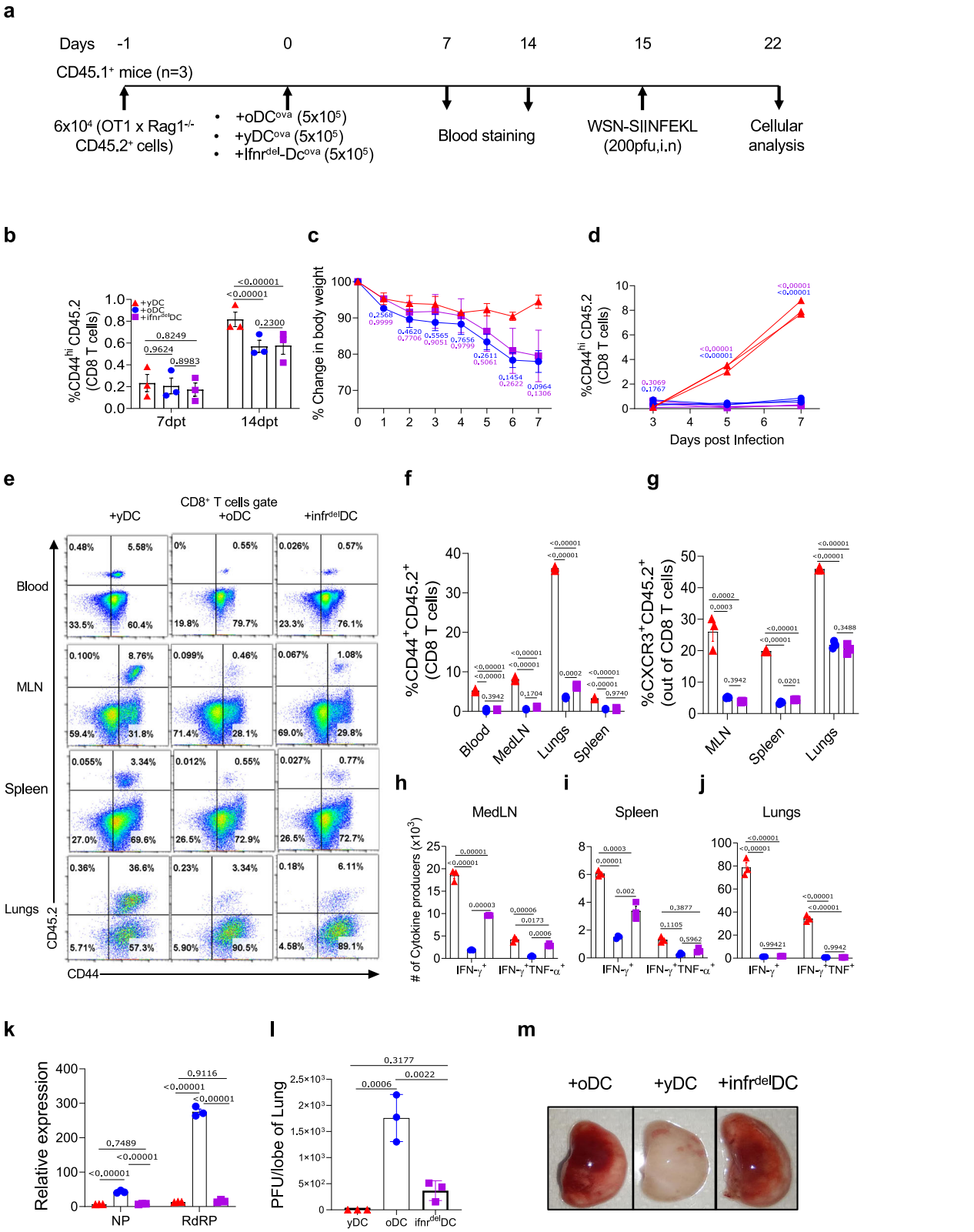

by CD8⁺ T cells that preferentially migrate to inflammatory tissues[34]. The SIINFEKL peptide-stimulated OT1 cells that produced IFN-γ or both IFN-γ and TNF were more frequent in the medLN (~2-fold), spleen (~1.5-fold) and Lungs (~8-fold) of animals receiving the Ova pulsed GM-CSF + IL-4 CD11c⁺CD11b⁺ cells of young as compared to those from aged mice (Fig. 3h–j). Significantly reduced titres of replicating IAV and less pronounced haemorrhagic and inflammatory lesions in the lungs of the animals were observed in the animals receiving the Ova pulsed GM-CSF + IL-4 CD11c⁺CD11b⁺ cells of young animals when compared with those receiving the cells of aged and ifnr^{del} mice (Fig. 3k–m). Therefore, DCs of aged or ifnr^{del} mice when compared with those of young animals generated reduced CD8⁺ T cell response and in doing provided poor protection against IAV.

Fig. 3 | Comparative assessment of young, aged and interferon receptor knockout (ifnr^{del}) BMDCs in priming CD8$^+$ T cell using DC immunisation. **a** BMDCs were in vitro differentiated from the bone marrow of young, aged and ifnr^{del} young mice. Equal numbers of FACS-sorted GM-CSF + IL-4 CD11c$^+$CD11b$^+$ cells were then pulsed with ovalbumin for 2 hours. The cells were washed 5 times with cold PBS to remove any soluble Ova protein and 5×10^5 cells were transferred into CD45.1$^+$ animals (+ oDC^{ova}: Aged DC recipients, +yDC^{ova}: young DC recipients, +ifnr^{del}DC^{ova}: ifnr^{del} DC recipients; n = 3/each group) which were previously infused with 6×10^4 OT1 cells/mouse. The recipients were then infected intranasally with an Influenza-A Virus (IAV, WSN-SIINFEKL) two weeks later to assess the OT1 response. **b** Bar diagrams summarise the frequency of expanded donor cells in the blood of the recipients at 7 and 14 days post BMDC transfer. Each point represents a biological replicate (n = 3). Data are shown as Mean ± SEM values and the levels of statistical significance were analysed by One-way ANOVA followed by Tukey Kramer post hoc test and the p-values are shown. **c** Line graph shows the change in body weights of different groups of animals at indicated days post infection (dpi). The levels of statistical significance were analysed by One-way ANOVA followed by Tukey Kramer post hoc test and the p-values are shown. p-values in blue colour are for the comparison between young and aged cell recipients whereas those in purple color are for comparison between young and ifnr^{del} cell recipients. **d** Line graph showing the kinetics of expanded virus-specific donor CD8$^+$ T cells in peripheral blood of recipients at different days post infection. The levels of statistical significance were analysed by One-way ANOVA followed by a Tukey Kramer post hoc test and the p-values are shown. **e** Representative FACS plot from different lymphoid and non-lymphoid organs show the distribution of specific donor cells. **f** Bar graphs show the frequencies of donor cells in different organs. **g** Bar graph depicts the frequency of CXCR3$^+$CD45.2$^+$CD8$^+$ T cells in different organs of BMDCs recipients. **h**–**j** ICCS assays were performed wherein cells from mediastinal LN (MedLN, **h**), spleen (**i**) and lungs (**j**) were stimulated with SIINFEKL-peptide to assess their functionality. Bar graphs show the number of indicated cytokine-producing cells. **k** Bar graph shows the viral load in the lungs of infected animals using influenza virus genes encoding for NP and RNA dependent RNA polymerase (RdRP) using specific primers. **l** Dot plots show the viral titres in the lungs as measured by plaque forming assays. For each group three biological replicates were used. **m** Representative images of lungs in each of the recipients are shown. The levels of statistical significance were analysed by One-way ANOVA followed by Tukey Kramer post hoc test and the p-values are shown. The data is representative of three individual replicates.

Rab8a overexpression restored compromised function in the aged DCs

Factors responsible for the differentiation of DCs from precursor cells engage CSF2Ra and IGFR. This results in the recruitment of a small GTPase, Rab8a and a subsequent activation of Akt via PI3K[35–37]. Compared with the cells of young mice, bone marrow cells of aged animals expressed significantly lower levels of *Csf2ra*, *Igf1r*, and *Rab8a* (Supplementary Fig. 9a–e). Similarly, the CD11c$^+$CD11b$^+$ enriched PBMCs of aged humans when compared with those of younger individuals also showed a lower expression of Rab8a (Supplementary Fig. 9f, g). We, therefore, reasoned that the reconstitution of Rab8a in DCs of aged host could improve functionality. Bone marrow cells of aged animals were genetically modified to overexpress Rab8a using a non-replicating lentivirus transduction approach. Control and the Rab8a reconstituted cells were then analysed (Supplementary Fig. 9h–k). The overexpression of Rab8a was established by qRT-PCR and western blotting (Supplementary Fig. 9j, k). FACS-sorted GM-CSF + IL-4 CD11c$^+$CD11b$^+$ cells of aged animals that were reconstituted of Rab8a upregulated *Akt1* (2-fold) and *Bcl2* (>3-fold) (Supplementary Fig. 9l, m). As these molecules are involved in nutrient sensing and cellular survival, their upregulation in the Rab8a reconstituted cells suggested for enhanced homoeostasis.

Next, we compared the transcriptome of splenic CD19^{-ve}CD3ε^{-ve} CD11c^{+ve}CD11b^{+ve} cells and GM-CSF + IL-4 CD11c$^+$CD11b$^+$ cells generated from aged and young mice. The RNAseq analysis also included the Rab8a overexpressing GM-CSF + IL-4 CD11c$^+$CD11b$^+$ cells of aged mice (Fig. 4a, b). We first compared the DEGs between the young and aged GM-CSF + IL-4 CD11c$^+$CD11b$^+$ cells with those of the splenic CD19^{-ve}CD3ε^{-ve}CD11c^{+ve}CD11b^{+ve} cells to establish the level of transcriptional similarity between the two cell types. Out of the 167 DEGs observed in the splenic CD19^{-ve}CD3e^{-ve}CD11c^{+ve} CD11b^{+ve} cells, 124 were also differentially expressed by GM-CSF + IL-4 CD11c$^+$CD11b$^+$ cells of aged and young mice. To prevent any confounding effects due to the lack of batch correction, we only compared the trend in the expression of these genes between the two cell types. Accordingly, the upregulated genes were assigned a value of 1 whereas the downregulated genes were assigned a value of 0. These values were then used to generate similarity matrices of the DEGs between the aged and young GM-CSF + IL-4 CD11c$^+$CD11b$^+$ BMDCs and CD19^{-ve}CD3ε^{-ve}CD11c^{+ve} CD11b^{+ve} splenocytes. Interestingly, 80.64% of the DEGs showing the reduced expression in the splenic cells of aged animals were also downregulated by GM-CSF + IL-4 CD11c$^+$CD11b$^+$ cells of aged animals (Fig. 4c). A similar trend was also evident for the upregulated genes, albeit with a lower similarity index of 61.95% (Fig. 4d). The overall similarity index was 70.94% (82/124 genes). Several antiviral genes such as *Oas2, Ifitm1, Ifit1, Ifit3* were downregulated, but *Arl4d* was upregulated in the GM-CSF + IL-4 CD11c$^+$CD11b$^+$ cells, a profile similarly observed for the CD19^{-ve}CD3ε^{-ve}CD11c^{+ve}CD11b^{+ve} splenocytes of aged compared to young mice. Some of the genes involved in innate immune functions showed discordance in the expression pattern within CD19^{-ve}CD3ε^{-ve}CD11c^{+ve}CD11b^{+ve} and GM-CSF + IL-4 CD11c$^+$CD11b$^+$ cells of aged and young animals which could be due to differences in the existing microenvironment. Therefore, despite differences in the transcriptome of splenic and BMDCs, the key genes responsible for their altered functionality in the aging animals showed a similar expression pattern within the two populations.

We then compared the whole transcriptome of aged, young, and Rab8a-OE GM-CSF + IL-4 CD11c$^+$CD11b$^+$ DCs by generating a heatmap of the log-normalised counts of the expressed genes. Interestingly, on a global level, the transcriptome of the Rab8a-OE GM-CSF + IL-4 CD11c$^+$CD11b$^+$ cells showed extensive similarity with that of the young GM-CSF + IL-4 CD11c$^+$CD11b$^+$ cells, indicating a 'reversal' of the immunosenescene in the aged DCs (Fig. 4e). A K-means clustering was also performed on the total transcriptome of aged, young and Rab8a-OE BMDCs to group the genes into clusters to ascertain the processes differentially regulated within each cell type (Supplementary Fig. 10). Cluster 0 and 1 remained unchanged within each group indicating the conservation of critical biological processes. Genes in cluster 2 that encoded for products involved in immune responses showed enhanced expression within the Rab8a-OE CD11c$^+$CD11b$^+$ DCs that was similarly observed in the cells of young animals. Therefore, the transcriptomic profile of the Rab8a reconstituted BMDCs of aged animals was similar to that of the cells from young animals.

Next, we proceeded with the phenotypic and functional characterisation of the Rab8a-OE GM-CSF + IL-4 CD11c$^+$CD11b$^+$ cells. The frequency of CD11b$^+$CD11c$^+$ cells and those expressing co-stimulatory molecules, CD80 and CD86, increased significantly within the Rab8a-OE cells as compared to the control (vector transduced) cells of aged mice (Fig. 5a–c, Supplementary Fig. 11a). Rab8a reconstitution also increased the frequencies of class I MHC expressing cells from 39% ± 0.75 to 64.53% ± 1.02 in the CD11c$^+$CD11b$^+$ BMDCs of aged animals (Fig. 5b, c, Supplementary Fig. 11a). We then assessed the IFN response of Rab8a overexpressing GM-CSF + IL-4 CD11c$^+$CD11b$^+$ cells following stimulation with either UV-inactivated or the replicating IAV. Rab8a-OE cells generated significantly improved IFN response as compared to the control cells of aged animals (Fig. 5d, e, Supplementary Fig. 11b–d). Accordingly, levels of *Ifna* (6.6-fold), *Ifnb* (11.6-fold), *Ifng* (16.6-fold), *Stat1* (24.4-fold), *Stat2* (41.6-fold) and anti-apoptotic molecule, *Bcl2* (35.7-fold) were increased in the Rab8a-OE cells compared to the

https://doi.org/10.1038/s41467-024-54757-2

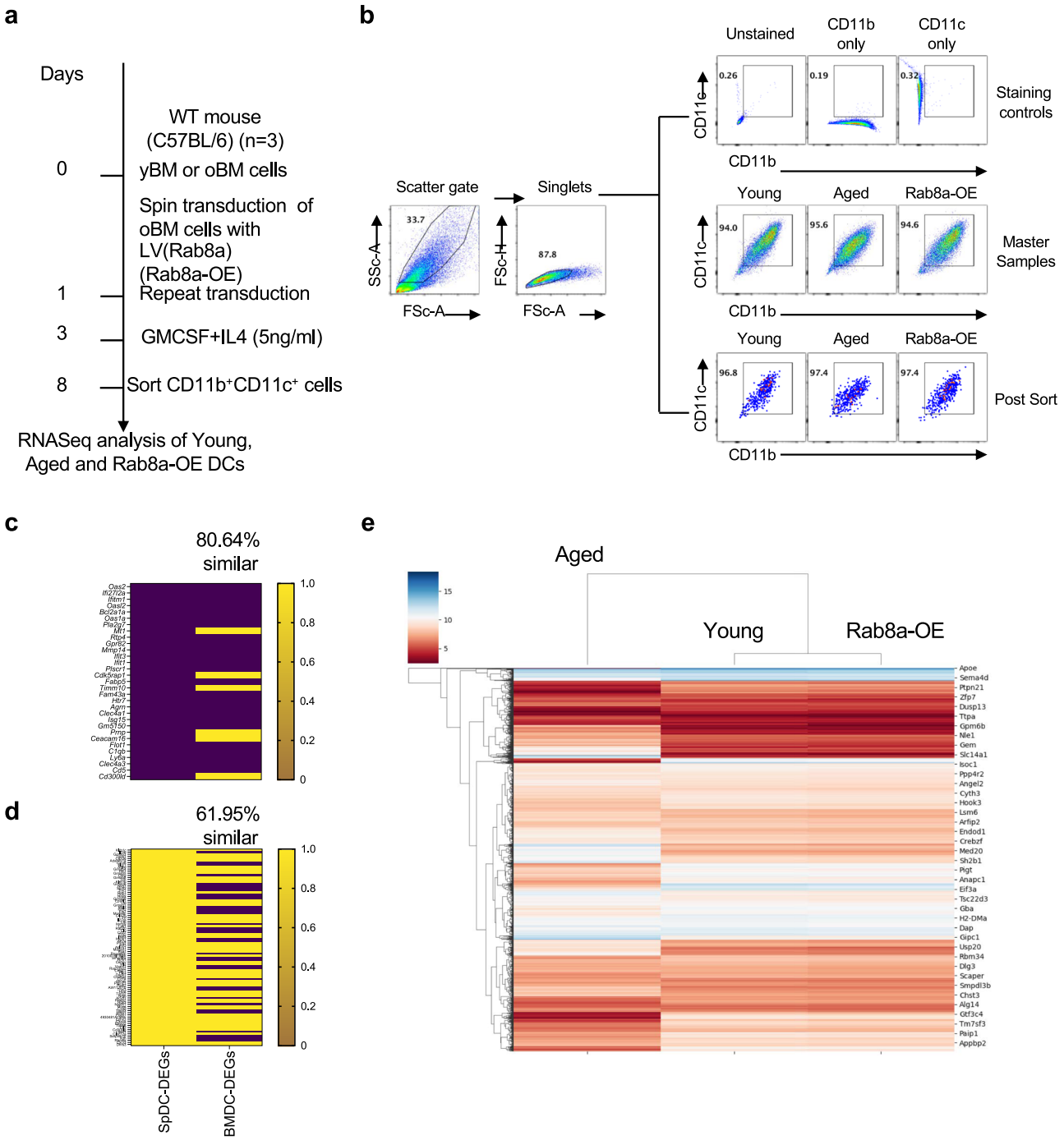

Fig. 4 | Transcriptomic analysis of young, aged and Rab8a overexpressing (Rab8a-OE) BMDCs. a A Schematic of experiments is shown. Bone marrow cells from aged mice were transduced to overexpress Rab8a. BMDCs were then generated by culturing the aforementioned cells in GM-CSF and IL-4 for 6 days. $CD11c^+CD11b^+$ cells were then FACS-sorted and RNAseq was performed to assess the transcriptome of the young, aged and Rab8a-OE BMDCs of aged animals. **b** The sorting strategy for purifying the GM-CSF + IL4 $CD11c^+CD11b^+$ BMDCs for RNASeq analysis of each group is shown. **c, d** The trend in DEGs between $CD3\varepsilon^{-ve}CD19^{-ve}CD11c^{+ve}CD11b^{+ve}$ splenocytes and GMCSF + IL4 $CD11c^+CD11b^+$ BMDCs was compared by generating similarity matrices. Similarity matrices summarising the downregulated DEGs (**c**) and upregulated DEGs (**d**) are shown. **e** A heatmap summarising the total transcriptome of each cell type is shown.

control aged cells (Fig. 5d, e). Similar results were also observed in the BMDCs pulsed with the inactivated viruses (Supplementary Fig. 11b–d). We then compared the potential of the aged, young, and Rab8a-OE GM-CSF + IL-4 $CD11c^+CD11b^+$ cells to activate $CD8^+$ T cells. The cells were fed with soluble Ova and subsequently co-cultured with CFSE labelled OT1 cells to measure proliferation. Whereas the GM-CSF + IL-4 $CD11c^+CD11b^+$ cells of young animals and the Rab8a-OE aged cells induced comparable expansion of OT1 cells, those of the aged mice did so poorly (Fig. 5f and g).

The differentiated GM-CSF + IL-4 $CD11c^+CD11b^+$ cells represented a heterogenous population (Supplementary Fig. 3b). We, therefore, measured the functionality of these cells following FCAS-depletion of NK cells and granulocytes ($NK1.1^-GR1^-$) or monocytes, granulocytes, and macrophages ($F4/80^-GR1^-$) (Supplementary Fig. 12a, b). Whether

https://doi.org/10.1038/s41467-024-54757-2

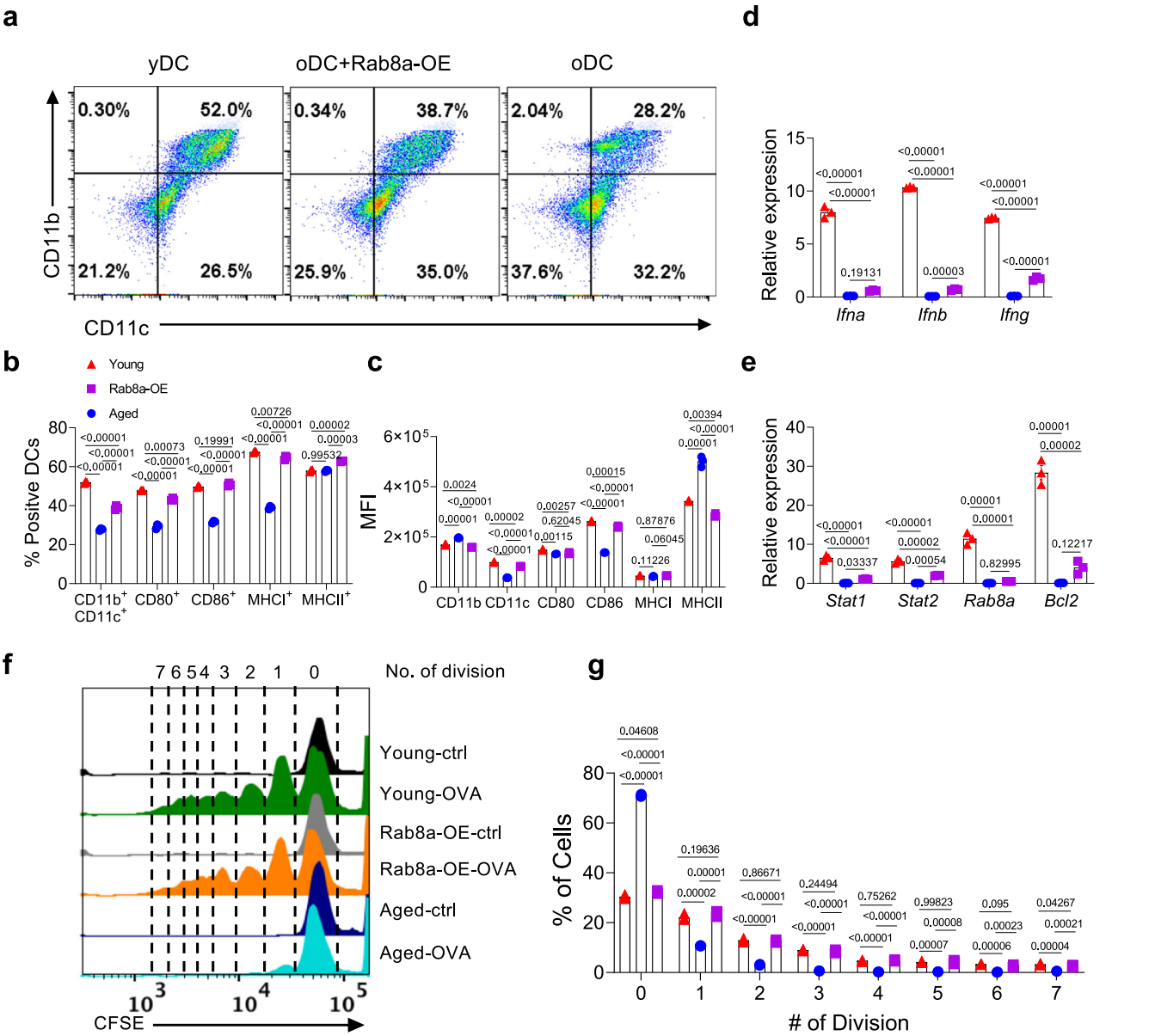

Fig. 5 | Rab8a influences the differentiation and functionality of DCs. **a** Representative FACS plots for analysis of CD11c$^+$CD11b$^+$ cells in each group are shown. **b**, **c** Phenotypic characterisation of BMDCs from different groups of cells is shown. The frequency (**b**) of the cells expressing the indicated markers and MFI values (**c**) for the markers are summarised as bar graphs. Three biological replicates were used for each condition. **d**, **e** Bar-graph show the expression of the key genes involved in type I IFN pathway in the GM-CSF + IL-4 CD11c$^+$CD11b$^+$ cells generated from young, aged and Rab8a-OE aged cells upon stimulation with IAV. Three technical replicates were used for each condition. **f**, **g** FACS-sorted GM-CSF + IL-4 CD11c$^+$CD11b$^+$ cells generated from young, aged and Rab8a-OE were pulsed with ovalbumin and then co-cultured with OT1 cells to measure their capability to stimulate OT1 cells. **f** Offset histograms show the extent of cell divisions in OT1 cells upon co-incubation. **g** Bar-graph depicts the frequency of CD8$^+$ T cells in each division. Three technical replicates were used for each condition. The data is representative of four individual replicates. The levels of statistical significance were analysed by One-way ANOVA followed by Tukey Kramer post hoc test and the p-values are shown.

Rab8a overexpressing cells of the aged mice (Rab8a-OE) regained functional competence was also assessed. The stimulated NK1.1$^-$GR1$^-$CD11c$^+$CD11b$^+$ cells of young animals showed enhanced *Ifna* expression which led to a higher fold-change between the cells of aged and young mice (Fig. 6a). Compared with the NK1.1$^-$GR1$^-$CD11c$^+$CD11b$^+$ cells of aged animals, the Rab8a overexpressing aged cells produced ~30, 10 and 5-fold higher levels of *Ifna*, *Ifnb* and *Ifng*, respectively (Fig. 6a). The elevated IFN response was evident in the unfractionated Rab8a overexpressing GM-CSF + IL-4 CD11c$^+$CD11b$^+$ cells, the NK1.1$^-$GR1$^-$ as well as F4/80$^-$GR1$^-$ CD11c$^+$CD11b$^+$ cells. Therefore, Rab8a reconstitution induced higher levels of IFNs in the aged BMDCs. Compared with the control cells, the Rab8a reconstituted GM-CSF + IL-4 CD11c$^+$CD11b$^+$ cells of aged mice expressed higher levels of several TLRs including those residing in endosomal membranes which might help explain the gain of functionality in the Rab8a reconstituted cells (Supplementary Fig. 5a–f).

The Ova pulsed unfractionated, NK1.1$^-$GR1$^-$ or F4/80$^-$GR1$^-$ GM-CSF + IL-4 CD11c$^+$CD11b$^+$ cells from all the three groups were also assessed for their ability to expand CFSE labelled OT1 cells (Fig. 6b, c). The OT1 cells undergoing more than three divisions were significantly higher in the co-cultures of Ova pulsed unfractionated DCs of young and Rab8a-OE aged animals than those obtained from the co-cultures of NK1.1$^-$GR1$^-$ or F4/80$^-$GR1$^-$ GM-CSF + IL-4 CD11c$^+$CD11b$^+$ cells of aged animals (Fig. 6c). While the contaminating F4/80$^-$GR1$^-$ cells

https://doi.org/10.1038/s41467-024-54757-2

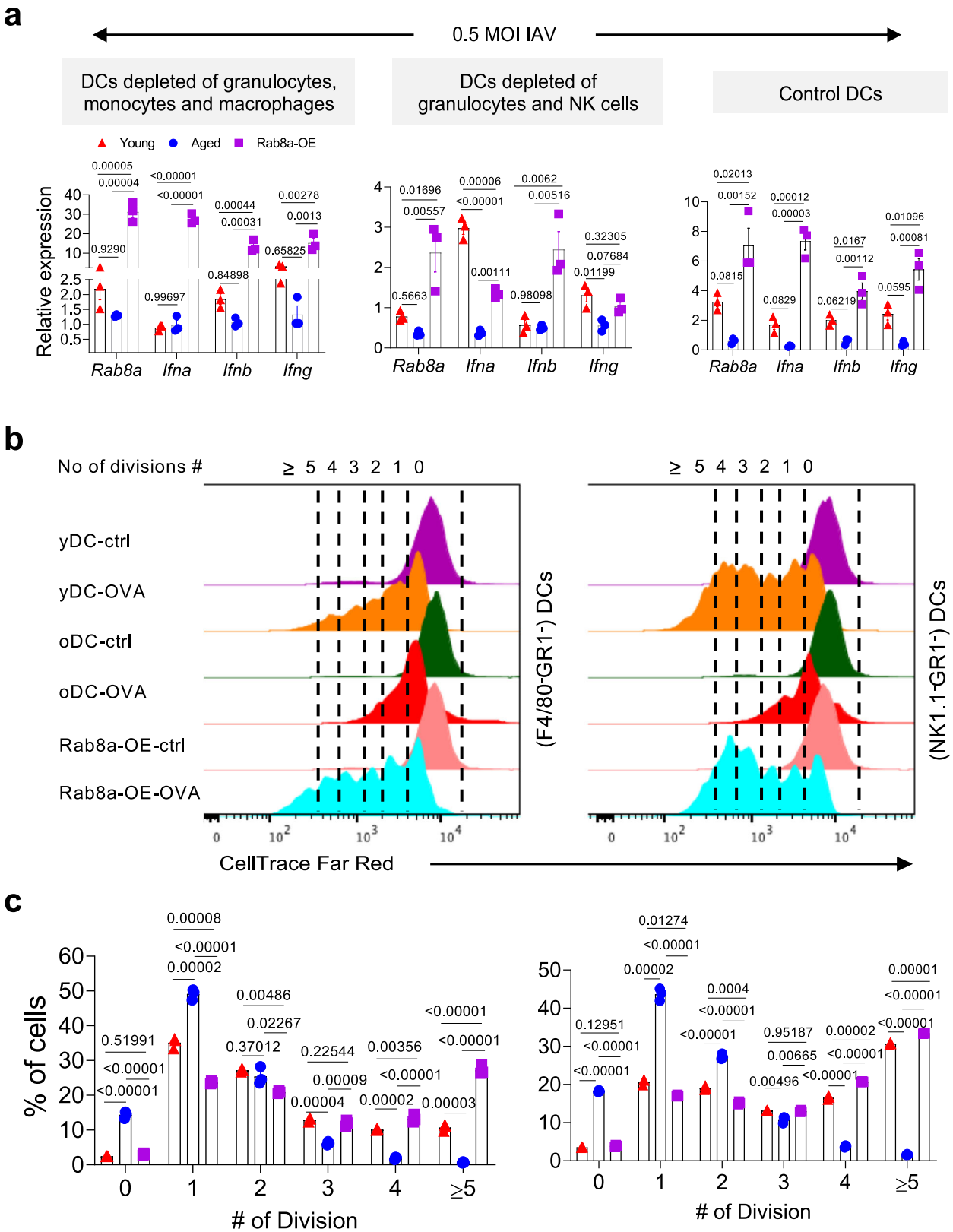

contributed to the observed effects in enhancing proliferative response of OT1 cells within the unfractionated GM-CSF + IL-4 $CD11c^+CD11b^+$ cells, DCs were primarily responsible for the age associated diminished innate immune functions. Furthermore, Rab8a reconstitution efficiently restored functionality in the aging cells.

We also assessed the cytokine production as well as T cell stimulating potential of FMS-like tyrosine kinase 3 ligand (Flt3l) induced BMDCs of aged and young animals (Fig. 7). Flt3l preferentially induces differentiation of conventional cDC1 population, a cell type that is known to efficiently cross prime $CD8^+$ T cells[38]. Rab8a reconstituted GM-CSF + IL-4 $CD11c^+CD11b^+$ cells and the Flt3l-$CD11c^+CD11b^+$ BMDCs of aged mice when stimulated with IAV produced significantly higher levels of IFNs (*Ifna, Ifnb*, and *Ifng*) as compared to the vector transduced control cells (Fig. 7a–e). Ova supplemented control and the

Fig. 6 | Assessing the functional contribution of contaminating monocytic (Ly6C), granulocytic (Ly6G), macrophages (F4/80) and NK (NK1.1) cells in GM-CSF + IL-4 BMDCs. Of the CD11c$^+$CD11b$^+$ DCs, the cells that were negatively stained for F4/80$^-$GR1$^-$ or NK1.1$^-$GR1$^-$ were sorted. Refer to supplementary Fig. 12 for the sorting strategy. **a** The sorted F4/80$^-$GR1$^-$CD11c$^+$CD11b$^+$, NK1.1$^-$GR1$^-$CD11c$^+$CD11b$^+$ DCs and the control CD11c$^+$CD11b$^+$ cells were pulsed with 0.5MOI of IAV for 3hrs and subsequently analysed for measuring the expression of the indicated genes by qRT-PCR. Unstimulated cells from each group were used as a control for normalisation of the expression data. **a** Bar graphs show the relative expression of the indicated genes in different conditions. For each group three technical replicates were used. **b, c** Representative offset histograms (**b**) and the bar graphs (**c**) show the frequencies of CFSE diluted OT1 cells that were co-cultured with F4/80$^-$GR1$^-$CD11c$^+$CD11b$^+$ or NK1.1$^-$GR1$^-$CD11c$^+$CD11b$^+$ cells that were supplemented with Ova for 2 hours. For each group three technical replicates were used. The experiments were repeated three times and representative data from one such experiment is shown. The levels of statistical significance were analysed by One-way ANOVA followed by Tukey Kramer post hoc test and the p-values are shown.

Rab8a reconstituted GM-CSF + IL-4 CD11c$^+$CD11b$^+$ or the Flt-3l CD11c$^+$CD11b$^+$ cell of aged mice were then assessed for their ability to stimulate OT1 cells. More than five divisions of the co-cultured OT1 cells were observed in the co-cultures of Rab8a reconstituted GM-CSF + IL-4 CD11c$^+$CD11b$^+$ or the Flt-3l CD11c$^+$CD11b$^+$ aged cell while the control cells induced only up to two divisions (Fig. 7f–k). An extended duration of Ova pulsing of Rab8a overexpressing GM-CSF + IL-4 CD11c$^+$CD11b$^+$ cells or the Flt3l-CD11c$^+$CD11b$^+$ DCs of aged animals did not significantly alter their ability to further expand OT1 cells when compared with the control cells of aged animals. The data showed that irrespective of the conditions used for their differentiation, BMDCs of the aged animals were inherently dysfunctional and that the Rab8a reconstitution restored diverse innate immune functions in such cells.

Given the critical role of the IGF1R-PI3K pathway in the differentiation of DCs, we depleted Rab8a in the cells of young animals using an shRNA approach to further elucidate its role (Supplementary Fig. 13a–d). Rab8a knockdown (KD) significantly reduced the expression *of Igf1r* (-30-fold) and a downstream kinase, *Akt1* (-17-fold) in GM-CSF + IL-4 CD11c$^+$CD11b$^+$ cells of young mice (Supplementary Fig. 13c). That the depletion of Rab8a downregulated the expression of *Igf1* was shown previously[39]. Rab8a depletion in the bone marrow cells of young animals reduced the frequencies of CD11c$^+$CD11b$^+$ BMDCs as well as those expressing CD80, CD86, class I and II MHC molecules when compared with the control cells of young animals when subjected to similar differentiation protocols (Supplementary Fig. 13e–j). Not only the differentiation but also the response to virus stimulation was reduced following Rab8a depletion in BMDCs of young animals. Accordingly, IAV-stimulated Rab8a depleted cells induced reduced expression of *Ifna* (70-fold), *Ifnb* (50-fold), *Ifng* 46-fold), *Stat1* (80-fold), and *Stat2* (4-fold) than the control cells (Supplementary Fig. 13k, l). Therefore, a reconstitution of Rab8a in CD11c$^+$CD11b$^+$ BMDCs of aged mice restores functionality and its depletion in the cells of young animals impedes differentiation program as well as their functional competence.

Rab8a reconstituted DCs promote in vivo CD8$^+$ T cell response via cross priming

The Rab8a reconstituted CD11c$^+$CD11b$^+$ BMDCs of aged mice regained ability to expand antigen-specific CD8$^+$ T cells. Since the surface display of peptide-MHC-I complexes by APCs is critical for engaging CD8$^+$ T cells, we measured such complexes (H-2K^b-SIINFEKL) in the SIINFEKL-peptide, or the Ova pulsed GM-CSF + IL-4 CD11c$^+$CD11b$^+$ cells. While a significant increase in the frequencies of H-2K^b-SIINFEKL positive CD11c$^+$CD11b$^+$ cells was observed in the Ova pulsed Rab8a reconstituted cells of aged mice as compared to the vector transduced control cells, such effects were milder in the SIINFEKL-peptide pulsed cells (Supplementary Fig. 14a, b). This suggested the role of Rab8a in preferentially enhancing antigen cross-presentation. We then captured initial events by measuring the conjugates of OT1 cells and Ova pulsed GM-CSF + IL-4 CD11c$^+$CD11b$^+$ cells of young, aged, and the Rab8a reconstituted aged cells (Rab8a-OE). GM-CSF + IL-4 CD11c$^+$CD11b$^+$ cells were FACS-sorted and labelled with Celltrace Far Red (CTFR). The cells were then pulsed with either SIINFEKL-peptide for 45 minutes or with Ova for 2hrs (Supplementary Fig. 14c, d). Thereafter, the cells were washed and co-incubated with CFSE labelled OT1 cells for 6 or 12hrs. The cells with dual staining for CTFR and CFSE were enumerated. The Rab8a-OE BMDCs as well as those of young animals formed such conjugates more frequently as compared to the cells of aged mice (Supplementary Fig. 14c, d). Therefore, in comparison to the control cells, the Rab8a-OE GM-CSF + IL-4 CD11c$^+$CD11b$^+$ cells of aged mice efficiently display H-2K^b-SIINFEKL complexes and efficiently engage with OT1 cells.

We, then tested whether the immune potentiating effects could be achieved in vivo with a 'DC therapy' using Rab8a-OE GM-CSF + IL-4 CD11c$^+$ cells of aged mice. A schematic of the experiments is shown in Fig. 8a. CD45.1$^+$ congenic animals previously infused with CFSE labelled OT1 cells (1×10^6) were intravenously injected with the Ova-pulsed FACS-sorted GM-CSF + IL-4 CD11c$^+$ cells of young, aged, and the Rab8a-OE cells of aged mice (Supplementary Fig. 15a, b). The recipients had an equal distribution of OT1 cells the following day of transfer (Supplementary Fig. 15a, lower panel). Three days later, the percentage of divided OT1 cells in the peripheral blood and splenic tissues of recipient animals of aged GM-CSF + IL-4 CD11c$^+$ cells were 33.3% and 25.3%, respectively (Fig. 8b, c). Up to a two-fold increase in the frequencies of OT1 cells was observed in peripheral blood and splenic tissues of the animals receiving the aged Rab8a-OE GM-CSF + IL-4 CD11c$^+$CD11b$^+$ cells (48.2% and 54.4%) and young GM-CSF + IL-4 CD11c$^+$ cells (47.5% and 36.1%) (Fig. 8b, c). The recipients of aged GM-CSF + IL-4 CD11c$^+$ cells had the lowest frequencies of OT1 cells while those receiving Rab8a-OE cells of aged mice, or young cells had up to 10-fold increase in the frequencies of OT1 cells in different lymph nodes (Fig. 8d and Supplementary Fig. 15c). In the same experiment, we also measured the frequencies of the transferred BMDCs (CD45.2$^+$CD11c$^+$ cells) in different groups to assess their homing potential. CD45.2$^+$CD11c$^+$ cells were more abundant in the peripheral blood than in the secondary lymphoid organs of the animals receiving GM-CSF + IL-4 CD11c$^+$ cells of aged animals as compared to those given the Rab8a-OE cells of aged mice or the young cells (Fig. 8e, f, Supplementary Fig. 15d, e). Chemokine receptors CCR7 and CCR5 govern homing of DCs. Lower frequencies of CCR7 expressing GM-CSF + IL-4 CD11c$^+$ cells were observed in aged compared to young as well as the Rab8a-OE cells of aged animals (Fig. 8f, Supplementary Fig. 15f, g). This could account for a poor homing of the aged DCs to secondary lymphoid organs[20]. The expanded OT1 cells and the distribution of Ova-pulsed GM-CSF + IL-4 CD11c$^+$CD11b$^+$ cells showed a direct correlation with the compartment having more DCs also showing the elevated T-cell response (Fig. 8d–f, Supplementary Fig. 15d-g). We also measured the expression of CCR7 in IAV-pulsed BMDCs, a situation more likely occurring in the infected host. GM-CSF + IL-4 CD11c$^+$CD11b$^+$ cells that expressed CCR7 were more frequent within the Rab8a-OE aged cells (37.50 ± 0.3%) and the cells of young animals (~ 41 ± 0.20%) as compared to those of the aged animals (26.5 ± 0.5%) (Fig. 8f, Supplementary Fig. 15d-h). Similar trends were observed for the expression of CCR5, a chemokine receptor that facilitates the migration of DCs to inflamed tissues (Fig. 8f). Flt3l CD11c$^+$CD11b$^+$ BMDCs preferentially home to secondary lymphoid tissues[40]. Ova-fed Flt3l CD11c$^+$CD11b$^+$ BMDCs from young, aged, or the Rab8a overexpressing cells were therefore transferred into sex-matched CD45.1$^+$ congenic young mice which had previously

https://doi.org/10.1038/s41467-024-54757-2

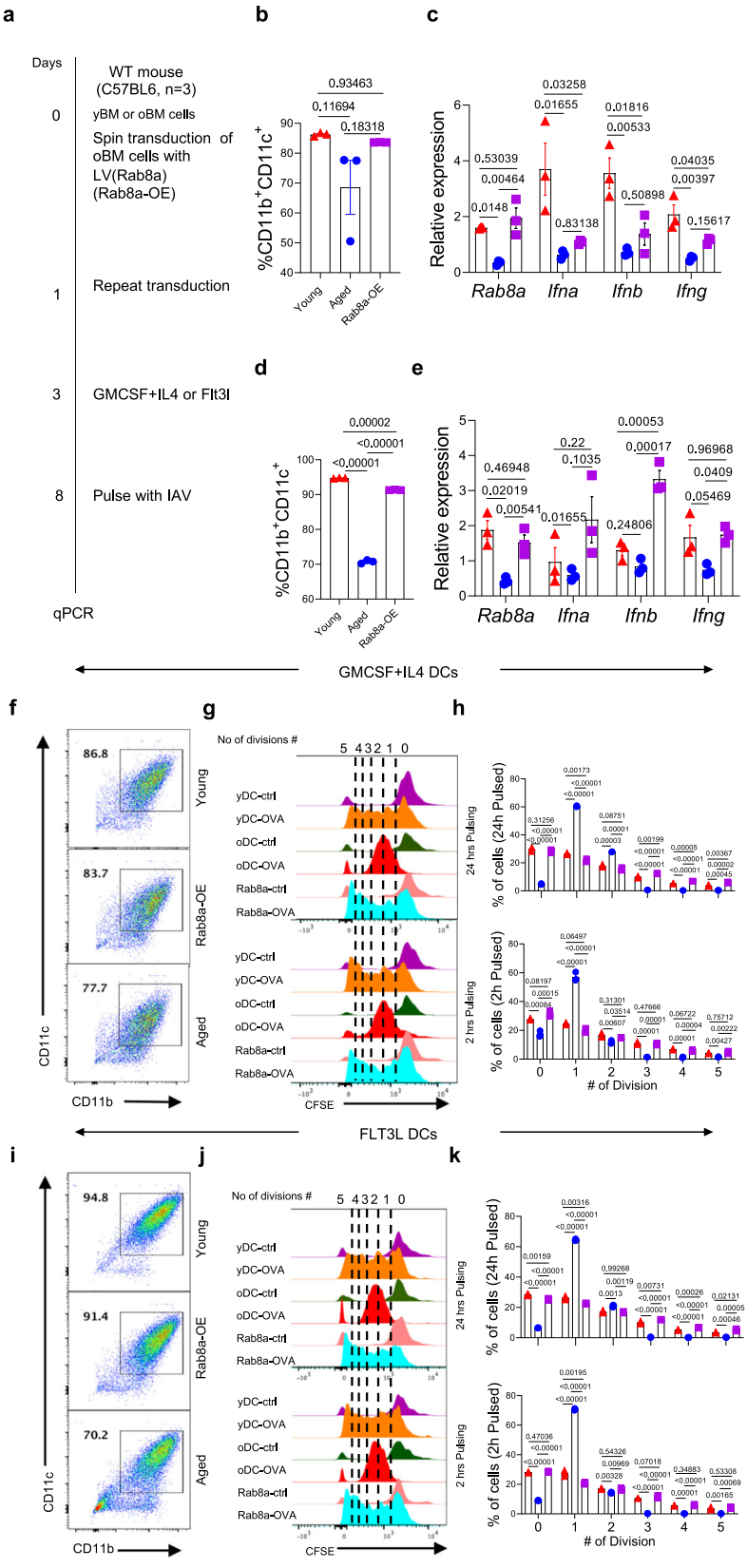

received CFSE-labelled OT1 cells. The proliferating donor OT1 cells were quantified three days later in the recipients. While a comparable CFSE dilution of OT1 cells was observed in the recipients of young and Rab8a overexpressing DCs, the animals receiving the cells of aged animals showed severely attenuated response of OT1 cells (Supplementary Fig. 16a–c). Therefore, like GM-CSF + IL-4 $CD11c^+CD11b^+$ cells, the Flt3l BMDCs of aged animals were greatly compromised in expanding T cells when compared with those of younger animals and their reconstitution with Rab8a enhanced functionality.

The data, therefore, showed that Rab8a overexpression in DCs of an aging host improved antigen cross-presentation to activate $CD8^+$ T cells in vitro as well as in vivo.

https://doi.org/10.1038/s41467-024-54757-2

Fig. 7 | A comparative analysis of the in vitro functionality of GM-CSF + IL-4 and Flt-3l induced BMDCs reconstituted of Rab8a. a A schematic of the experiment is shown. Young, aged and Rab8a-OE bone marrow cells were cultured for 6 days with either GM-CSF/IL-4 or Flt3l. The cells were then functionally characterized. **b** The frequencies of GMCSF + IL4 $CD11c^+CD11b^+$ cells in each group are shown. For each group three technical replicates were used. **c** The generated GM-CSF + IL4 $CD11c^+CD11b^+$ cells were pulsed with 0.5MOI of IAV and the transcript abundance for the indicated genes were measured via qRT-PCR. Bar diagrams show the relative expression of the indicated genes. For each group three technical replicates were used. **d** The frequencies of Flt3l $CD11c^+$DCs in each group are summarized. Three technical replicates were used for each group. **e** The generated Flt3l $CD11c^+CD11b^+$DCs were stimulated with 0.5MOI of IAV and the transcript abundance for the indicated genes were measured via qRT- PCR. Bar diagrams show the relative expression of the indicated genes. Three technical replicates were used for each condition. **f**,**g** In a separate set of experiments, the generated GMCSF + IL4 BMDCs or the Flt3l BMDCs were pulsed with Ova for 2- and 24-hrs and were then co-cultured with CFSE labelled OT1 cells for 72 hrs. **f** Representative FACS plots show the frequencies of GM-CSF + IL4 $CD11c^+CD11b^+$ cells in each group. **g** Representative offset histograms show the frequencies of CFSE diluting OT1 cells co-cultured with ova pulsed GM-CSF + IL4 $CD11c^+CD11b^+$ cells as indicated. **h** Bar graphs show the frequencies of CFSE diluted cells within each division of CFSE diluted OT1 cells. Three technical replicates were used for each condition. **i** Representative FACS plots show the frequencies of Flt3-l DCs in each group. **j** Representative offset histograms show the frequencies of CFSE diluting OT1 cells co-cultured with ova pulsed Flt3l-$CD11c^+$ DCs in indicated conditions. **k** Bar graphs show the frequencies of CFSE diluted cells within each division of CFSE diluted OT1 cells. Three technical replicates were used for each condition. The experiments were performed four times and data from one such experiment is shown. The levels of statistical significance were analysed by One-way ANOVA followed by Tukey Kramer post hoc test and the p-values are shown.

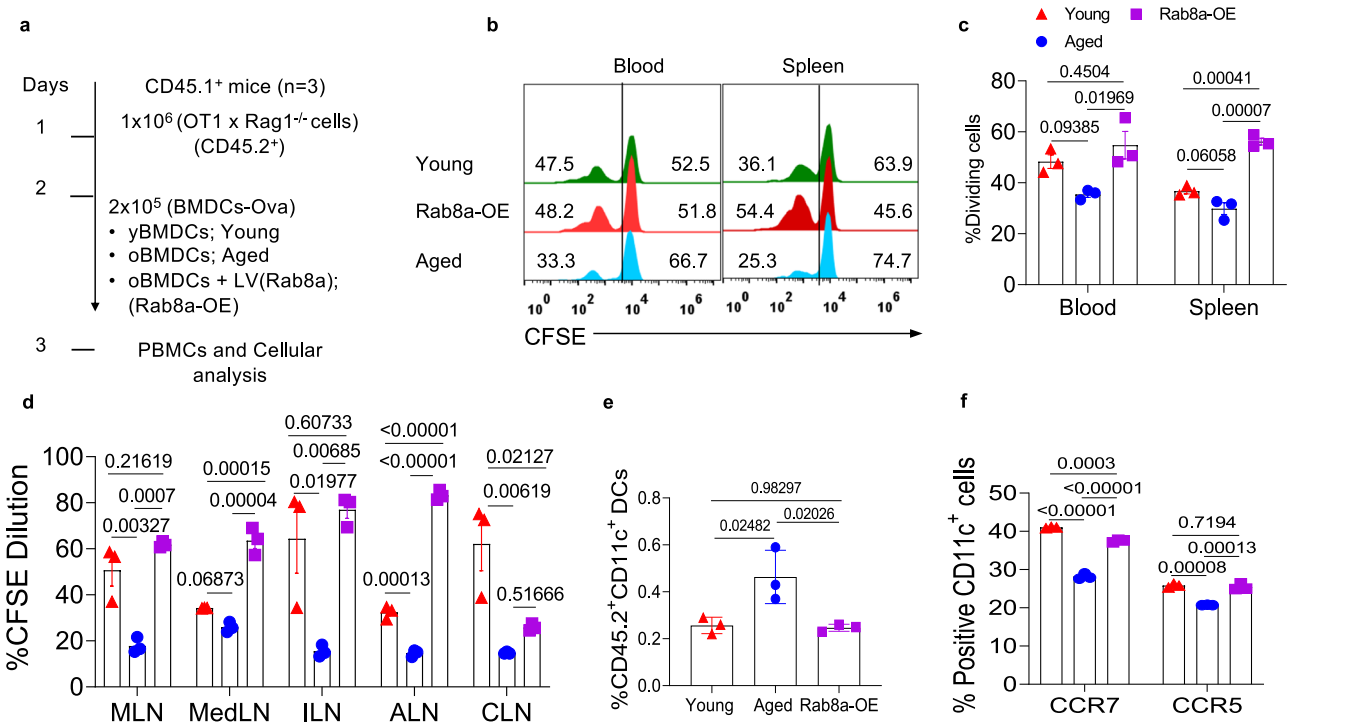

Fig. 8 | Comparative assessment of in vivo antigen presentation capability of young, aged and Rab8a-OE GM-CSF + IL-4 $CD11c^+CD11b^+$ BMDCs. In vivo antigen presentation by young, aged and Rab8a-OE GM-CSF + IL-4 $CD11c^+CD11b^+$ cells from was performed. **a** A schematic of the experiments is shown. 2×10^5 Ova pulsed FACS-sorted GM-CSF + IL-4 $CD11c^+CD11b^+$ cells generated from young, aged and Rab8a-OE bone marrow cells were transferred into $CD45.1^+$ animals which were previously infused with 1×10^6 CSFE labelled OT1 cells. 72hrs post transfer of BMDCs, the animals were euthanized and the expansion of the donor $CD8^+$ T cells was measured. **b** Representative offset histograms show the frequency of divided OT 1 cells in peripheral blood and spleen. **c** Bar graphs show the frequencies of divided OT 1 cells. Three biological replicates were used for each group. **d** Bar graphs show the percentage of OT1 cells that have atleast undergone one division in the indicated LNs. (MLN: Mesenteric, MedLN: Mediastinal, ILN: Inguinal, ALN: Axillary, CLN: Cervical). Three biological replicates were used for each condition. **e** Bar graphs show the percentage of $CD45.2^+CD11c^+$ donor BMDCs in the peripheral blood of recipients. Three biological replicates were used for each condition. **f** Bar graph shows the frequency of $CCR5^+CD11c^+$ and $CCR7^+CD11c^+$ BMDCs generated from different conditions. Three biological replicates were used for each group. The experiments were repeated three times and representative data from one of the experiments is shown. Data represent Mean ± SEM values. The levels of statistical significance were analysed by One-way ANOVA followed by Tukey Kramer post hoc test and the p-values are shown.

Rab8a reconstituted DCs generate effective antigen-specific memory $CD8^+$ T cell response

Whether the expanded $CD8^+$ T cells by Rab8a reconstituted GM-CSF + IL-4 $CD11c^+CD11b^+$ cells of an aged host generate memory cells was investigated. The schematic of the experiments is shown in Fig. 9a. In vivo expanded OT1 cells by Ova-fed GM-CSF + IL-4 $CD11c^+CD11b^+$ cells of young, aged and the Rab8a overexpressing cells of aged animals were longitudinally tracked (Fig. 9a). Compared with the control cells of aged mice, Rab8a-OE aged GM-CSF + IL-4 $CD11c^+CD11b^+$ cells or the cells of young mice induced >3-fold increased response of OT1 cells in peripheral blood of the recipients at 3- and 6-days post transfer (Fig. 8b–d, Supplementary Fig. 17a–d). The expanded cells were allowed to further differentiate into memory cells for a month and subsequently recalled by infecting animals with IAV (WSN-SIINFEKL). Animals receiving DCs of young animals or the Rab8a reconstituted aged cells when compared with the recipients of aged cells reduced their body weights to a lesser extent (Supplementary Fig. 17e). At 6 dpi, the expanded donor $CD44^+CD45.2^+$ $CD8^+$ T cells were up to a 10-fold

https://doi.org/10.1038/s41467-024-54757-2

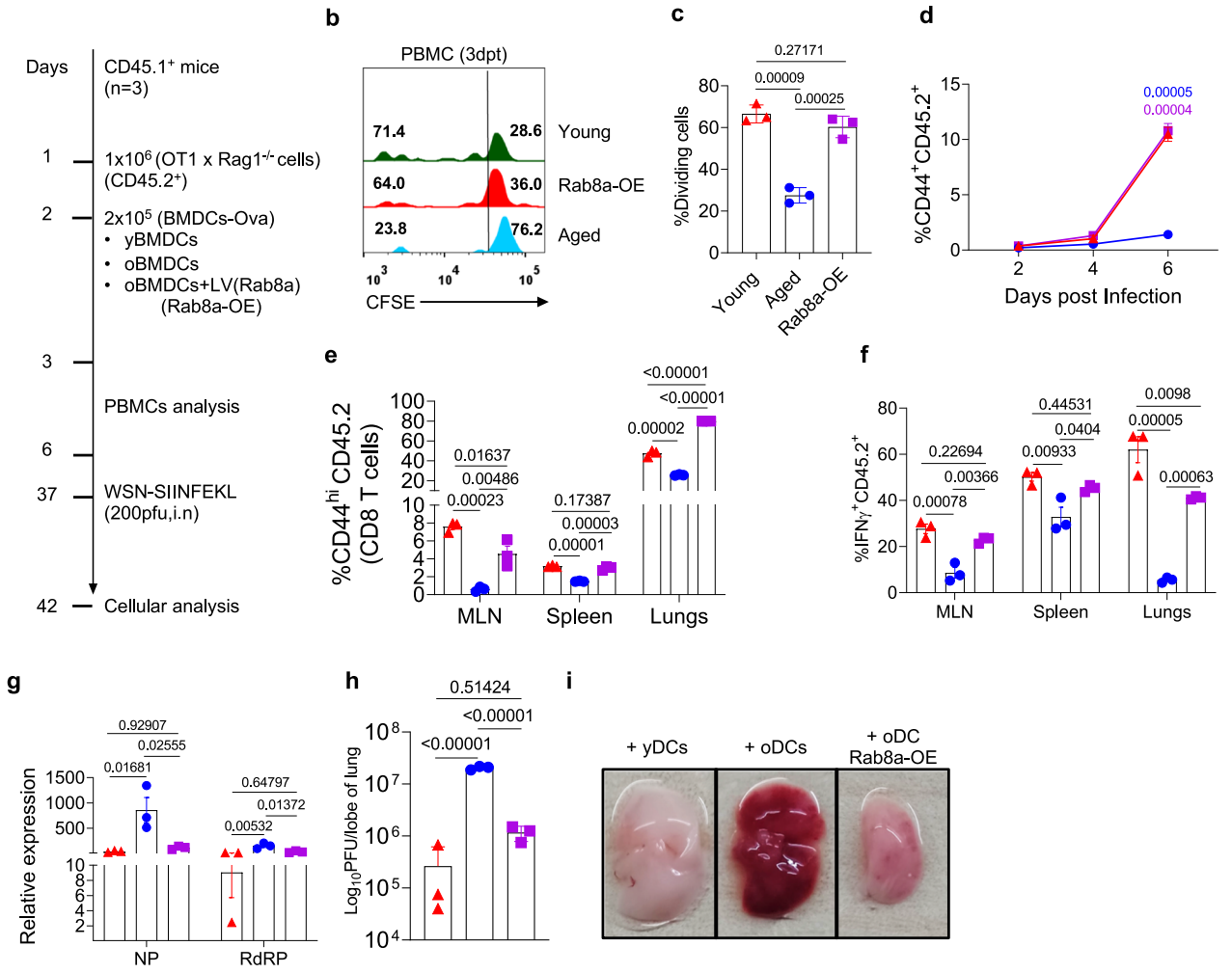

Fig. 9 | Rab8a reconstituted BMDCs generate efficient memory CD8⁺ T cells. a A schematic of the experiments is shown. In-vitro generated GM-CSF + IL-4 CD11c⁺CD11b⁺ cells from young, aged and Rab8a-OE bone marrow cells were FACS-sorted and pulsed with Ova for 2hrs. After extensive washings, 2×10^5 of the GM-CSF + IL-4 CD11c⁺CD11b⁺ cells were adoptively transferred into sex matched CD45.1⁺ congenic animals that were previously infused with 1×10^6 of CFSE labelled OT1 cells. The expansion of donor OT1 cells was then analysed in the acute phase in the peripheral blood and following a challenge with IAV (WSN-SIINFEKL) to recall memory cells. **b** Representative offset histograms show the expansion of the transferred CFSE labelled CD8⁺ T cells at 3 days post transfer of BMDCs. **c** Bar graphs show percentage of divided cells. Three biological replicates were used for each group. **d** Line diagrams show the kinetics of expanded antigen-specific donor OT1 cells in the peripheral blood of recipients post WSN-SIINFEKL infection. Three biological replicates were used for each group. Data is represented as Mean ± SEM and the levels of statistical significance were analysed by One-way ANOVA followed by Tukey Kramer post hoc test and the p-values are shown. **e** Bar graphs show the frequency of expanded OT1 cells in the mediastinal LN (MLN), spleen and lungs of WSN-SIINFEKL infected mice. Three biological replicates were used for each group. **f** Bar graphs show the frequencies of IFN-γ⁺ cells following SIINFEKL-peptide stimulation as assessed by ICCS assays. Three biological replicates were used for each condition. **g** Bar graphs show viral load in lung tissues of the infected group of animals as measured by quantifying the mRNA of IAV genes encoding nucleoprotein (NP) and RNA dependent RNA polymerase (RdRp) specific primers. $n = 3$ biological replicates. Data is represented as Mean ± SEM and the levels of statistical significance were analysed by One-way ANOVA followed by Tukey Kramer post hoc test and the p-values are shown. **h** Dot plot shows the viral titres in infected lungs as measured by plaque forming assays. $n = 3$ biological replicates. Data is represented as Mean ± SEM and the levels of statistical significance were analysed by One-way ANOVA followed by Tukey Kramer post hoc test and the p-values are shown. **i** Representative images of lungs from each group show haemorrhagic lesions in the each group of the recipients. The experiments were repeated three times and representative data from one such experiment is shown.

more in the peripheral blood of animals receiving Rab8a-OE cells or the young DCs in comparison to those injected with the aged GM-CSF + IL-4 CD11c⁺CD11b⁺ cells (Fig. 9d). Frequencies of OT1 cells were 0.64%, 4.34%, and 7.87% in medLN, 1.46%, 3.06% and 3.3% in spleens and 25.70%, 80% and 48.70% in lungs of the animals receiving DCs from aged, Rab8a-OE and young animals, respectively (Fig. 9e, Supplementary Fig. 17f). The cytokine production by SIINFEKL-peptide stimulated donor OT1 cells was assessed by ICCS assays. IFNγ⁺CD8⁺ T cells were 7.58%, 23.56% and 28.8% in medLN, 29.43%, 51.9% and 45.42% in spleens and 5.66%, 41.81% and 67.7% in lungs of the animals receiving the DCs from aged, the Rab8a-OE and the young animals, respectively (Fig. 9f, Supplementary Fig. 17g–i). Similar results were obtained for IFN-γ⁻TNF⁺ and IFN-γ⁺TNF⁺ double positive OT1 cells from different groups (Supplementary Fig. 17g–i). Viral loads were reduced by >100-fold in the recipients of Rab8a-OE DCs than those receiving control cells of aged animals (Fig. 9g, h). Similarly, haemorrhagic lesions in the lungs were less evident in the recipients of Rab8a-OE DCs than those receiving the aged DCs (Fig. 9i). Additionally, Flt3l-CD11c⁺CD11b⁺ cells from young, aged, and Rab8a-OE conditions were pulsed with Ova and adoptively transferred into sex-matched CD45.1⁺ congenic mice which previously received OT1 cells. The persisting memory cells were recalled a month later via intranasal WSN-SIINFEKL infection (Supplementary Fig. 18a). Significantly increased frequencies of the expanded OT1 cells were observed in the recipients of

Flt3l-BMDCs of young and the Rab8a reconstituted aged DCs than in the animals injected with the aged cells (Supplementary Fig. 18a–d). ICCS assay also revealed significantly higher frequencies of IFN-γ producing donor cells in lungs and spleen of animals receiving Rab8a-OE Flt3l-DCs than in the recipients of control aged cells (Supplementary Fig. 18e–g).

Therefore, Rab8a reconstituted DCs of aged animals efficiently primed $CD8^+$ T cells which helped control IAV during reinfection.

Rab8a promotes survival and differentiation of aging DCs via mTOR pathway

We investigated molecular events modulated by Rab8a in bone marrow cells during differentiation process to generate BMDCs (Supplementary Fig. 19a). Rab8a-depleted bone marrow cells of young animals had significantly reduced expression of *Igf1r* and *Pi3kca* which are involved in cellular growth and survival (Supplementary Fig. 19b). A significantly reduced expression of *Akt1, Akt2*, and *Akt3* was also observed in the Rab8a-depleted cells (Supplementary Fig. 19c). However, the expression levels of *Tsc1* and *Tsc2* were significantly increased in the Rab8a depleted BMDCs (Supplementary Fig. 19d). We also analysed the genes of mTOR pathway such as mTORC1, and the components of mTORC2 such as *Rictor, Raptor*, and *Sin1* as well as that of *Rps6kb1*, a positive regulator of cellular growth and survival. Rab8a knockdown in the BMDCs of young animals reduced the expression of these genes while the Rab8a reconstitution increased their expression (Supplementary Fig. 19d–i).

To measure the protein expression of key genes involved in the differentiation BMDCs, the cell lysates were analysed by immunoblotting. Depletion of Rab8a was confirmed using anti-Rab8a antibody (Supplementary Fig. 19j). While the baseline expression of Akt1 and its phosphorylated version (pAkt1) were higher in the bone marrow cells of young as compared to those of aged animals, the expression further increased in the differentiated BMDCs (Supplementary Fig. 19j). Following Rab8a depletion, both Akt1 and pAkt1 were downregulated by bone marrow cells as well as BMDCs (Supplementary Fig. 19k). An earlier study showed that the knockdown of Rab8a did not alter the expression of Akt1 and reduced the levels of pAkt1 in TLR4 ligand induced macrophages[41]. The differential activation status of BMDCs following GM-CSF + IL-4 supplementation in comparison to a more inflammatory milieu generated due to TLR signalling could account for the observed effects. Rab8a reconstituted bone marrow cells upregulated the expression of both Akt1 and pAkt1 in steady state as well as following differentiation into BMDCs (Supplementary Fig. 19j). The expression levels of Akt1 and pAkt1 were also quantified by flow cytometry (Supplementary Fig. 19k–p). BMDCs of young animals expressed increased levels of Akt1, pAkt1 as well as Rab8a than the cells of aged mice (Supplementary Fig. 19k and n). Rab8a reconstituted BMDCs of aged animals upregulated both Akt1 and pAkt1while its genetic depletion in the cells of young animals reduced the expression (Supplementary Fig. 19l–p). Taken together, the expression data showed that the reconstitution of Rab8a promoted cellular growth and survival via activation of mTOR pathway.

Rab8a controls the turnover of class I MHC molecules to enhance antigen presentation

Rab8a reconstituted BMDCs showed elevated surface display of peptide-class I MHC complexes and preferentially expanded $CD8^+$ T cells. Such effects could be due to a differential trafficking pattern of class I MHC molecules following Rab8a overexpression. Rab8a localises to different cellular compartments such as plasma membrane[42], macropinosomes[43], recycling endosomes[44], microtubules and pseudopodia as well as the exocytic vesicles. Rab8a is also essential for the fusion of exocytic vesicles to the plasma membrane[45]. Furthermore, an overexpression of Rab8a promotes cell protrusion and dorsal ruffles as well as membrane trafficking[43,46]. Therefore, we reasoned that Rab8a could modulate the surface expression of membrane proteins including MHC molecules in DCs. We performed confocal analysis of Ova pulsed or the control BMDCs of young, aged and the Rab8a reconstituted BMDCs of aged animals. We observed a significant increase in the expression of Rab8a in Ova pulsed BMDCs of young mice but with slower kinetics in those of aged mice (Fig. 10a, b, Supplementary Fig. 20a). Rab11 preferentially localizes in ERCs where class I MHC molecules accumulate[12]. Rab8a overexpressing aged BMDCs significantly upregulated Rab11 and the levels further increased upon Ova supplementation (Fig. 10a, b, Supplementary Fig. 20a). Both Rab8a and Rab11 showed a significantly higher co-localisation in BMDCs of young and Rab8a-OE-aged cells than in the control cells of aged mice (Fig. 10c and Supplementary Fig. 20a). Therefore, Rab8a reconstituted DCs of aged animals were enriched in ERCs which might facilitate the efficient trafficking of class I MHC molecules to the plasma membrane. We then measured H-$2K^b$-SIINFEKL complexes in the ERCs following Ova feeding. While the un-pulsed BMDCs showed no staining for H-$2K^b$-SIINFEKL, the Ova-pulsed cells showed substantially higher staining (Fig. 10c and Supplementary Fig. 20a). BMDCs of young and the Rab8a reconstituted cells of aged mice showed significantly higher levels of H-$2K^b$-SIINFEKL than the control cells of aged mice (Fig. 10c and Supplementary Fig. 20a). H2-K^b-SIINFEKL efficiently colocalized with Rab8a and Rab11 in the Ova-pulsed BMDCs of young and Rab8a-OE BMDCs when compared with the cells of aged mice (Fig. 10c and Supplementary Fig. 20a). Analyses using immunoblotting and flow cytometry demonstrated an increased expression of Rab8a and Rab11 in the Ova fed BMDCs of young and aged animals following Rab8a reconstitution (Fig. 10d–f and Supplementary Fig. 20b–d). We conclude that Rab8a in conjunction with Rab11 induces efficient transports of H-$2K^b$-SIINFEKL complexes to ERCs for their enhanced surface display in the Ova fed BMDCs. It was shown previously that Rab8a colocalised with Rab11 and Rab22a and that their expression pattern corelated with enhanced cross-presentation[44,45]. Taken together the data show that Rab8a reconstituted DCs of aged mice efficiently displayed p-MHC molecules to activate $CD8^+$ T cells.

We observed an altered morphology of antigen-pulsed BMDCs generated from the aged mice while no such differences were evident in the cells of young or the Rab8a-OE aged cells (unpublished observation). Such alteration could be driven by differential actin polymerisation, a highly energy-dependent process[47]. We performed intracellular staining with Phalloidin-AF488 to quantify the actin content in the cells. Frequencies of phalloidin positive cells were ~27%, 43.2% and ~60%, in the GM-CSF + IL-4 $CD11c^+CD11b^+$ cells of aged, young and the cells of aged animals that overexpressed Rab8a, respectively (Fig. 10g–i). Earlier reports showed the formation of cell protrusion and dorsal ruffle in the cells overexpressing Rab8a[48]. Therefore, Rab8a reconstitution of GM-CSF + IL-4 $CD11c^+CD11b^+$ cells of aged mice improved their morphological features which could promote migratory potential. A recent study demonstrated the role of the cell shape in improving the functionality of DCs[49]. This issue however needs further investigation in the DCs of aged animals.

Since the aged population exhibits higher susceptibility to infection and responds poorly to vaccination, it becomes imperative to devise immune potentiating strategies for this demographic group[50,51]. We investigated the molecular intricacies associated with the compromised functionality of DCs in the aging host and observed their poor anti-viral IFN response and impaired antigen presentation. Highly reduced levels of Rab8a in splenic DCs and BMDCs of aged animals led us to investigate its role in DCs' biology using overexpression and genetic depletion studies. Rab8a-depleted bone marrow precursors of young animals were compromised in differentiating into DCs while those of aged animals following Rab8a overexpression did so efficiently (Supplementary Fig. 21). Furthermore, Rab8a reconstituted BMDCs showed enhanced cytokine production, improved homing

https://doi.org/10.1038/s41467-024-54757-2

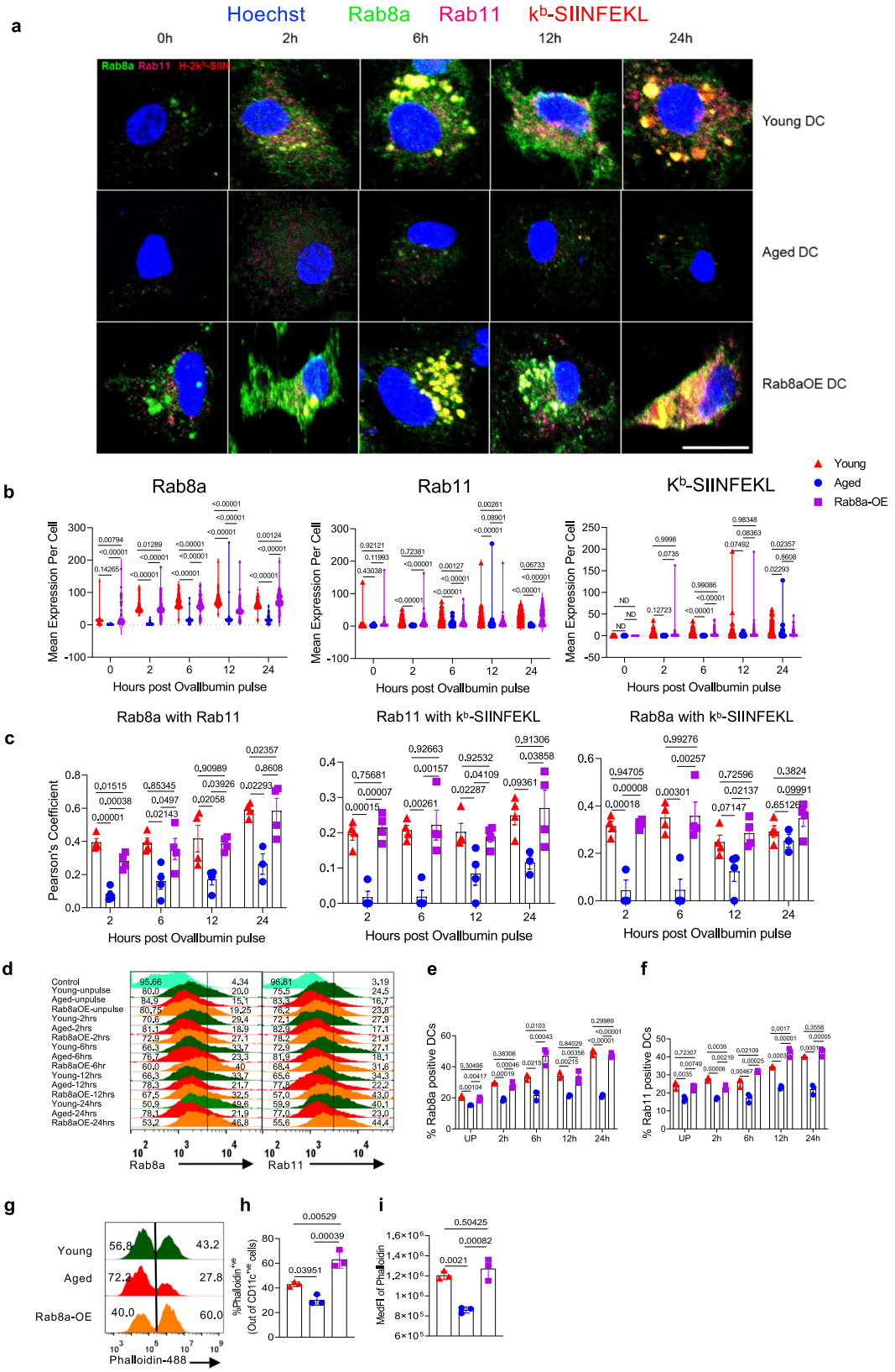

potential, and efficiently engaged with CD8⁺ T cells (Supplementary Fig. 21). These observations, therefore, could have implications not only in managing viral infections but also in enhancing the efficacy of vaccines as well as in improving anti-tumour response in the aging population. DCs intrinsically are short-lived cells and the 'empowered DCs' could efficiently expand CD8⁺ T cells, a fraction of which forms persisting memory to provide lasting protection. Therefore, 'empowered DCs' when used as cell-based therapies may not pose long-term toxic effects unlike those resulting from genetic modification of persistent adaptive immune cells. While elaborate mechanistic details are yet to be investigated, our observation that Rab8a critically controls the functionality and differentiation of DCs and its reconstitution in

Fig. 10 | Rab8a promotes antigen-processing and presentation by GM-CSF + IL-4 CD11c$^+$CD11b$^+$ BMDCs of aged animals by efficiently displaying peptide-MHC I complexes. a Confocal microscopic images show the expression of Rab8a, Rab11 and H-2K^b-SIINFEKL when GM-CSF + IL-4 CD11c$^+$CD11b$^+$ cells from young, aged and the cells of aged animals following Rab8a overexpression (Rab8a-OE) pulsed with Ovalbumin for indicated time points. Scale bar = 10μm. **b** Plots showing the cumulative data for mean expression levels of Rab8a, Rab11 and H-2K^b-SIINFEKL. (The exact number of cells used for analysis are indicated within the source data file). **c** The colocalization of different molecules was measured by Pearson's coefficient in GM-CSF + IL-4 CD11c$^+$CD11b$^+$ cells of each group following ovalbumin stimulation for the indicated time points. A total of 4 fields with at least 50 cells were analysed for colocalization. The experiments were performed three times and data from one such experiments are shown as Mean ± SEM values. **d** Representative offset histograms show the intracellular expression levels of Rab8a and Rab11 in the permeabilized GM-CSF + IL-4 CD11c$^+$CD11b$^+$ cells which were fed with Ova as indicated. **e** Bar graphs show Rab8a expressing GM-CSF + IL-4 CD11c$^+$CD11b$^+$ cells. Three technical replicates were used for each condition. **f** Bar graphs show Rab11 expressing GM-CSF + IL-4 CD11c$^+$CD11b$^+$ cells. Three technical replicates were used for each condition. **g** Offset histogram show the frequency of phalloidin-AF488 positive GM-CSF + IL-4 CD11c$^+$CD11b$^+$ BMDCs from each group. **h** Bar graph show cumulative data for frequencies of phalloidin-AF488 positive cells. **i** MFI values for phalloidin-AF488 are shown in the GM-CSF + IL-4 CD11c$^+$CD11b$^+$ cells in the indicated conditions. Three technical replicates were used for each condition. The experiments were repeated three times and data from one such experiment is shown as Mean ± SEM values. The levels of statistical significance were analysed by One-way ANOVA followed by Tukey Kramer post hoc test and the p-values are indicated.

the DCs of aging host might represent a viable option to potentiate immune function.

Methods

Mice, viruses, and cell lines

Wild type C57BL/6 (Stock #000664), IFNR-KO (B6.Cg-Ifngr1tm1Agt Ifnar1tm1.2Ees/J; Stock #029098), OT1 (C57BL/6-Tg (TcraTcrb) 1100Mjb/J; Stock #003831) and B6 CD45.1 (B6.SJL-Ptprc^a Pepc^b/BoyJ; Stock #002014) mice were obtained from Jackson Laboratory, USA and bred and housed in individual ventilated cages at the barrier facilities in the Small Animal Facility for Experimentation (SAFE), IISER Mohali. All the animal experiments were conducted strictly adhering to the approved protocols by the institutional animal ethics committee (IAEC) of IISER Mohali. Mice were euthanized using CO_2 for further analysis. Female mice were used for all the experiments. The young mice were 6-8 weeks, and the aged mice were >18 months old. MHV68-SIINFEKL and IAV-WSN-SIINFEKL were grown and titrated using Vero and MDCK cells, respectively[52,53].

Ethics statement for human study

All the work with humans was approved by the institute ethics committee (IEC/2022/05) of the Indian Institute of Science Education and Research. All the recruited volunteers provided written informed consent.

Antibody and other reagents

Antibodies used for measuring the expression of different molecules were obtained from BD biosciences, eBiosciences and BioLegend. The antibodies were against CD11c-PE-Cy7 (Biolegend, N418, 1:300, Cat. No. 117318), CD11c-PE (Biolegend, N418, 1:300, Cat. No. 117308), CD11b-FITC (Biolegend, M1/70, 1:400, Cat. No. 101206), CCR5-PE-Cy7 (Biolegend, HM-CCR5, 1:400), CCR7-APC (Biolegend, 4B12, 1:200, Cat. No.), CD80-PE (Biolegend, 16-10A1, 1:400, Cat. No. 104708), CD86-APC (Biolegend, GL-1, 1:400, Cat. No. 105012), GR1-APC (Biolegend, RB6-8C5, 1:500, Cat. No. 108412), NK1.1-PE-Cy7 (Biolegend, S17016D, 1:500, Cat. No. 156514), F4/80-PE (BD Biosciences, T45-2342, 1:400, Cat. No. 565410), CD8-PerCP-Cy5.5 (Biolegend, 530-6.7, 1:200, Cat. No. 100734), CD44-APC (Biolegend, IM7, 1:400, Cat. No. 103012), CD45.2-FITC (Biolegend, 104, 1:200, Cat. No. 109806), CD45.2-PE (Biolegend, 104, 1:200, Cat. No. 109808), CXCR3-FITC (Biolegend, CXCR3-173, 1:200, Cat. No. 126536), TNF-APC (Biolegend, TN3-19.12, 1:500, Cat. No. 506108), IFNγ-PE (Biolegend, XMG1.2, 1:500, Cat. No. 505808), MHCI-APC (Biolegend, 28-8-6, 1:500, Cat. No. 114614) MHCII-APC (Biolegend, M5/114.15.2, 1:500, Cat. No. 107614) H-2K^b-SIINFEKL-PE (BD Biosciences, 25-D1.16, 1:500, Cat. No. 569792), Ly6C-PerCP-Cy5.5 (Biolegend, HK1.4, 1:500, Cat. No. 128012), Ly6G-PE (Biolegend, 1A8, 1:300, Cat. No. 127608) and anti-human CD11c-APC (BD pharmingen, Cat 559877, 1:500). CFSE (Carboxyfluorescein succinimidyl ester, Cat. No. C34554) and Cell-Trace Far Red (Cat. No. C34572) to label the live CD8$^+$ T cells and BMDCs respectively were obtained from Invitrogen. PI staining was also performed to assess the cellular viability. Phalloidin-AF488 (A12379, Invitrogen) was used for actin staining. Anti-mouse-GAPDH (GA1R, Cat. No. MA5-15738, Invitrogen), anti-Akt (Cell Signalling Technology, 40D4, Cat. No. 2920), anti-pAkt1 (Cell Signalling Technology, D25E6, Cat. No. 13038), anti-Rab11 (Cell Signalling Technology, D4F5, Cat. No. 5589), anti-mouse-Rab8a (Invitrogen, 261CT1.3.1, Cat. No. MA5-24717) were used for western blotting. The anti-mouse Alexa-Flour568 was from invitrogen (Cat. No. A11004). GM-CSF (Cat. No. 315-03, Peprotech) and IL-4 (Cat. No. 214-14, Peprotech) were used in complete RPMI-1640 (Cat. No. 61870036, Gibco) media supplemented with 10% FBS (A5256701, Gibco) and Penicillin-Streptomycin (Cat. No. 10378016, Gibco) for differentiation of BMDCs. HEK293T, Vero E6, and MDCK cells were maintained in 10% DMEM (Cat. No. 11965092, Gibco). Lentiviruses for knockdown (Rab8a-shRNA) and overexpression (Rab8a-OE) of Rab8a were generated using HEK293T cells and concentrated using PEG-NaCl (20% PEG-8000 and 1.2 M NaCl).

In vitro BMDC generation

Young (6-8 weeks old), aged (> 18 months old) wild-type and IFNR-KO (6-8 weeks old) female mice were euthanized to isolate bone marrow cells. Long bones such as femur and tibia were flushed with 10% RPMI-1640. The prepared single cell suspensions were RBC lysed using 1x RBC lysis buffer (155 mM NH_4Cl, 12 mM $NaHCO_3$, 0.1 mM EDTA, pH 7.3). 15×10^6 of the bone marrow cells were then re-suspended in 15 mL of 10% RPMI supplemented with 5 ng/mL of GM-CSF and IL-4 and seeded in a 100 mm petri dish for 6 days in a humidified CO_2 incubator. Half of the culture medium was replaced with complete RPMI supplemented with 5 ng/ml of IL-4 and GM-CSF every alternate day. The cultured cells were harvested after five days using a cell scrapper and washed twice with 10% RPMI at 4 °C for 5 minutes at 200xg. The viability of the in-vitro generated BMDCs was assessed using trypan blue staining. For some experiments, 20 ng/mL of Flt3l (Peprotech) was used for generating BMDCs from young, aged, and Rab8a-OE expressing bone marrow cells of aged mice. These cells were used for further in vitro and in vivo analysis.

Sample preparation for RNA-seq analysis

Aged ($n = 10$, >24 months old) and young ($n = 8$, 6-8 weeks old) female mice were used for isolating the CD11c$^+$CD11b$^+$ cells from splenic tissues of both groups. Spleen from young and aged animals were collected in 10% RPMI. The splenic tissues were chopped into pieces using scissors and were treated with liberase (60U/ml) for 15 minutes at 37 °C. Thereafter, the cell suspensions were prepared by gently crushing them in a 70μm cell strainer using the soft side of a 2 mL syringe plunger. The cell suspension from each group was centrifuged at 250 g for 5 minutes and the supernatant was discarded. The cells were re-suspended in RBC lysis buffer for 5 minutes at room temperature (25 °C) for RBC lysis and then centrifuged at 250 g for 5 minutes. After that cells were washed twice using 1x-PBS (pH 7.4) and finally resuspended in 10% RPMI and were stained with antibodies against CD19, CD3e, CD11b, and CD11c for 30 minutes on ice. The

stained cells were washed twice with 10% RPMI and finally, the $CD19^-CD3e^-CD11c^+CD11b^+$ cells were FACS purified. The purity of the sorted cells was ascertained to be more than 95%. 1×10^6 of the sorted cells from each sample were stored in RNA later (Invitrogen, AM7021) at -80 °C. The cells were processed for RNA isolation using a kit from Qiagen.

Additionally, BMDCs generated from young (8 weeks), aged (18 months) and the cells of aged (18 months) female mice reconstituted of Rab8a (Rab8a-OE) were FACS sorted based on the expression of $CD11c^+CD11b^+$ staining (GM-CSF + IL-4 $CD11c^+CD11b^+$ cells) from five replicates of each condition. The cells were kept at -80 °C in Trizol and the RNA isolation was done using the Trizol method.

RNA sequencing and differential gene expression

A total of 1 µg RNA was subjected to RNA sequencing. cDNA library preparation from the RNA samples was done using Illumina TruSeqSample Preparation protocols. The generated cDNA libraries were sequenced using the Illumina Hi-Seq-2000 platform. The data generated was analyzed by Tuxedo protocol and the raw reads in FAST-Q format were aligned to the reference genome of *Mus musculus* (mm9) using Tophat. Only high-quality reads with a QC score of more than 20 were used for alignment. Further data analysis was performed as explained earlier[46]. To generate a list of differentially expressed genes (DEGs) a cutoff value of 5 RPKM for either condition was used. Thereafter, 1.5-fold change (young vs aged) in the expression was set to classify DEGs (Supplementary Fig. 1a).

For the RNAseq analysis of BMDCs, the sequenced raw data were processed to obtain high quality clean reads using Trimmomatic v0.39 to remove the adapter sequences, ambiguous reads (reads with unknown nucleotides "N" larger than 5%), and low-quality sequences (reads with more than 10% quality threshold (QV) < 25 phred score). A minimum length of 100 nt (nucleotide) after trimming was applied. After removing the adapter and low-quality sequences from the raw data, high quality reads were obtained. These high quality (QV > 25), paired-end reads were used for reference based read mapping. The high-quality reads of the samples were mapped on the reference genome using STAR (v 2.7.10a) with default parameters. FeatureCounts (version 2.0.3) was used to count the read numbers mapped on each gene. The log normalised counts were then generated. Additionally, for performing K-means clustering for differential biological process analysis, the formatted.csv files for the mapped counts for each gene in the samples were imported as a dataframe in a python environment and the fragments per kilobase of transcript per million mapped reads (FPKM) was calculated for all the genes. The gene expression values were then scaled using 'MinMaxScaler' from the scikit-learn package and then the 'KMeans' module was used to identify different clusters of genes within each sample. This was followed by K-means clustering. Seaborn and matplotlib were used for plotting the data.

Functional annotation and network analysis of differentially expressed genes in DCs of aged mice

RNA-seq data was generated as described earlier[52]. DEGs obtained selected using the above-mentioned threshold values were used for further analysis. The functional annotation and gene ontology was performed using the WEB-based Gene SeT AnaLysis Toolkit (Webgestalt, (http://webgestalt.org/option.php) using the *Mus musculus* genome as a reference. All the DEGs were used as input for network analysis using the STRING database (Search Tool for the Retrieval of Interacting Genes, https://string-db.org/). All the networks were generated using STRING default parameters[52].

Knockdown and overexpression of Rab8a in bone marrow cells

For the knockdown of Rab8a in the bone marrow of female young (6-8 weeks) WT C57BL/6 mice, shRNA sequences for Rab8a and scramble control were designed using default settings on www-data@wi.mit.edu site. The oligos were cloned into a modified pLKO.1-GFP RNAi cloning vector. The primers used are mentioned in Supplementary table 1. For generating lentiviruses, 100-mm petri-dish seeded with HEK293T cells at 80% confluency were co-transfected with 5 plasmids, *viz*. 10 µg Rab8a shRNA/scrambled construct, 9.8 µg pCMVR8.74 (packaging vector), 6 µg pMD2.G (envelope vector), 6 µg Tat and 6 µg Rev plasmids. The transfection mixture was prepared by mixing the plasmids in 1 mL of serum-free DMEM containing poly ethylenimine (PEI) in a 1:3 ratio (DNA: PEI). The mixture was immediately vortexed for 20 seconds and then incubated at room temperature for 15 minutes. Thereafter, the transfection mixture was overlaid carefully onto HEK293T cells, and plates were kept in a humidified CO_2 incubator for 6 hours. Subsequently, the media was replaced with 10% DMEM and plates were left in a CO_2 incubator for 72 hours. Transfection of HEK293T cells was analysed by visualising the expression of GFP. The supernatants were collected 72 hours post-transfection and centrifuged at 200 g to remove cell debris. The assembled lentiviruses were then concentrated using PEG-NaCl. The concentrated lentiviruses were used for the knockdown of Rab8a using spin transduction and the efficiency of transduction was measured using flow cytometry. Knockdown was confirmed by western blotting and qRT-PCR[54].

The Rab8a gene was cloned using *XbaI* and *BamHI* sites in the pLenti-GFP vector for overexpression in the bone marrow cells of aged mice. Lentivirus generation and concentration were performed as described above. Rab8a expression levels were measured by western blotting, qRT-PCR, and fluorescent microscopy.

Flow cytometric analysis

Peripheral blood samples were collected in 1.5 mL of micro-centrifuge tubes containing 10 µL of 500 mM EDTA. 35 µL of the blood samples were taken and incubated with 7 µL of antibody mix for 30 minutes on ice. The red blood cells were then lysed by adding 400 µL of RBC lysis buffer (155 mM NH_4Cl, 12 mM $NaHCO_3$, 0.1 mM EDTA, pH 7.3). The cells were analysed flow cytometrically using a BD C6 Flow cytometer or FACSAria Fusion.

For surface staining of the cells, different organs were harvested in 10% RPMI, and single-cell suspensions were prepared using a 70 µm strainer and gently crushing them using the soft end of a 2 mL syringe plunger. RBC lysis was performed for splenic and bone marrow cells. The cells were stained using the indicated antibodies on ice for 30 minutes. The cells were then washed by centrifugation at 200 g for 5 minutes in 1xPBS at 4 °C and acquired using a BD C6 flow cytometer. For surface staining of immune cells from lungs, the tissue was first digested with collagenase (0.5 mg/mL) for 1 hr at 37 °C. The single-cell suspensions were then prepared and the cells were stained using the indicated fluorescent antibodies at 4 °C for 30 minutes.

For phenotyping of the in-vitro generated BMDCs, cells were gently removed from the culture plates using a cell scrapper and washed twice in complete RPMI by centrifugation performed at 200 g for 5 minutes at 4 °C. The staining was performed as described above. The splenic DCs were similarly phenotypically characterized[55].

For the intracellular cytokine staining (ICCS) assays, an equal number (5×10^5) of cells from different organs were pulsed with 10 µg/mL of $Ova_{257-264}$ (SIINFEKL-peptide) for 4 hours at 37 °C in the presence of 1x Brefeldin A. The cells were then surface stained and treated with IC fixation buffer (ebioscience, Cat. No. 88-8824-00) for 30 minutes on ice. The cells were permeabilized using an IC permeabilization buffer for 15 minutes. The intracellular cytokine staining was then performed by incubating the cells for 45 minutes with the antibody cocktail prepared in the permeabilization buffer on ice. The cells were washed twice with 1xPBS and acquired using a BD C6 flow cytometer.

For sorting BMDCs, in-vitro generated GM-CSF + IL-4 or Flt3l induced BMDCs were harvested and washed twice in 10%RPMI. The

cells were then incubated with the antibody cocktail for 30 minutes on ice. Subsequently, the cells were washed and sorted based on CD11b and CD11c staining using BD FACSAria Fusion III. Additionally, for the depletion of macrophages, neutrophils and NK cell population from the $CD11b^+CD11c^+$ cells, in-vitro generated BMDCs were stained with antibodies against mouse CD11b, CD11c, F4/80 and GR1 (Ly6G/Ly6C) or NK1.1 and GR1. The stained cells were sorted for $NK1.1^-GR1^-CD11b^+CD11c^+$ or $F4/80^-GR1^-CD11b^+CD11c^+$ cells for further analysis.

The expression of Rab8a along with Akt1 and pAkt1 was measured in the bone marrow cells and BMDCs flow cytometrically. First, the cells were surface stained with antibodies against CD11c and CD11b. The cells were then fixed and permeabilized using IC fixation and permeabilization buffer and stained using anti-CD16/32 antibodies for blocking Fc receptors. The primary antibodies against Akt1 and p-Akt1 were then added for 30 minutes at room temperature. The cells were then washed, and the bound primary antibodies were then probed with Alexa-Fluor 568 tagged secondary antibodies. A similar analysis was performed for the Rab8a overexpressing or the shRNA knocked down (KD) bone marrow cells or the BMDCs. A similar approach was employed to detect the expression of Rab8a and Rab11 in the Ova pulsed BMDCs generated from young, aged, and Rab8a overexpressing BM cells of aged mice.

qRT-PCR for measuring the mRNA expression levels of different genes

PBMCs collected from humans, bone marrow cells or the FACS-sorted $CD11b^+CD11c^+$ cells from BMDCs of young or aged mice were stimulated with either 0.5 MOI live or UV-inactivated Influenza-A Virus (IAV-WSN-SIINFEKL) or γ-herpesvirus (MHV-68-SIINFEKL) for three different time points (30 minutes, 3hrs and 6hrs). The unstimulated cells from each group were used as control for normalisation of the expression data. At the indicated time points, RNA was isolated using Trizol. The concentration and the quality of the RNA preparation were assessed using OD_{280} and $OD_{260/280}$ measurements, respectively. An equal concentration of RNA was then used for synthesising cDNA using a verso cDNA kit (Thermo Fisher Scientific). qPCR was then performed using a 2X-DyNamo ColorFlash SYBR Green qPCR kit (ThermoFisher). The relative expression of HPRT or 18 s rRNA measured for different samples served as the endogenous control for estimating the abundance of transcript using $2^{-\Delta\Delta CT}$ method[56].

To measure type I IFN response, in-vitro generated BMDCs ($CD11b^+CD11c^+$) from young (~ 6-8 weeks old) and aged (> 18 months old) female mice were FACS-sorted. An equal number of the sorted DCs were then pulsed in vitro with 0.5 multiplicity of infection (MOI) of IAV (WSN-SIINFEKL) or MHV68-SIINFEKL for different time intervals (30 minutes, 3hrs and 6hrs). RNA was then isolated from the collected cells at the indicated time and cDNA was synthesised. The expression of genes of IFN pathway was measured by qRT-PCR as described above. Human blood samples were collected from 06 young (~ 25 years) and 06 aged (~ 65 years) healthy donors in EDTA containing tubes. PBMCs were isolated using histopaque. Equal numbers of the isolated PBMCs or $CD11c^+CD11b^+$ enriched cells were pulsed with 0.5MOI of IAV for 30 minutes, 3hrs, and 6hrs. The cells were then harvested for RNA isolation and analysed by qRT-PCR for measuring the expression of different genes involved in the IFN pathway. The primers used for the expression analysis are mentioned in Tables S2–S4.

Bone marrow cells of young mice were subjected to shRNA-mediated knockdown of Rab8a by spin transduction with lentiviruses containing the Rab8a shRNA constructs. The cells were then used for generating BMDCs by culturing them in media supplemented with 5 ng/mL GM-CSF and IL-4. Five days later, the cells were harvested and an equal number of the sorted cells were pulsed with 0.5MOI of IAV for 6 hours. The cells were processed for RNA isolation to measure the expression of different genes by qRT-PCR. BMDCs generated from scrambled control transduced BM cells served as controls for normalisation.

In a separate experiment, Rab8a was overexpressed in the bone marrow cells of aged mice by transducing with pseudotyped replication incompetent lentiviruses containing the Rab8a construct. The transduced cells were then used for generating BMDCs by culturing them in media supplemented with GM-CSF and IL-4 for 5 days. Equal number of the FACS-sorted $CD11c^+CD11b^+$ BMDCs were then pulsed with 0.5MOI of either live or UV-inactivated IAV for 6 hours. The cells were then used for RNA isolation followed by cDNA preparation. qRT-PCR was performed to measure the expression of various genes. BMDCs from aged and young animals were also generated for comparison. For assessing the kinetics of expression of genes encoding for IGF1R and Rab8a, bone marrow cells from young and aged mice were cultured in the presence of 5 ng/mL of IL-4 and GM-CSF for 12, 24, and 48 hrs. At the indicated time points, the cells were isolated to prepare RNA samples. qRT-PCR was performed using the converted cDNA to measure the abundance of different transcripts. In separate experiments, the FACS-depleted DCs were pulsed with 0.5MOI of IAV and the expression of Rab8a along with IFNα, IFNβ, and IFNγ were measured. To analyse the expression of Rab8a and the interferon genes such as *Ifna*, *Ifnb*, and *Ifng* from bonafide conventional DCs ($CD11b^+/CD11c^+$), Flt3l was used to their differentiation. Such cells were then stimulated with the viruses as described earlier.

Antigen presentation assay

In-vitro generated BMDCs of young (6-8 weeks) and aged (> 18 months) female animals were FACS-sorted using anti-CD11b and anti-CD11c antibodies as double-positive cells. The sorted BMDCs were then pulsed with 25 µg/mL of $Ova_{257-264}$ (SIINFEKL) for 45 minutes or 200 µg/mL of chicken ovalbumin (Ova) for 2 or 24hrs. Subsequently, the cells were washed twice using complete RPMI. These cells were used for co-culture with CFSE-labelled OT-I cells from sex matched mice to assess the expansion of the Ova reactive $CD8^+$ T cells. The cells were washed twice with 1xPBS and stained with anti-CD8 antibody after 72 hours of co-culture. The stained samples were acquired using a BD Accuri C6 flow cytometer and the data was analysed using FlowJo (BD Biosciences) software. Additionally, the DCs depleted of NK cells, macrophages were also pulsed with ovalbumin and co-cultured with CellTrace Far Red™ labelled OT1 cells to assay priming potential.

DC immunisation experiments

In-vitro generated BMDCs ($CD11b^+$ and $CD11c^+$) from young (6-8 weeks), aged (> 18 months), and IFNRKO (6-8 weeks old) female mice were FACS-sorted. The sorted BMDCS were washed once with complete RPMI and equal numbers of cells from each group were pulsed with Ova (200 µg/ml) for 2 hrs. The cells were then washed thrice with 1xPBS and adoptively transferred into young (6-8 weeks old) $CD45.1^+$ female mice that were previously infused with OT1 cells of young (6-8 weeks old) female mice. The frequency of OT-I cells was checked in the peripheral blood of the recipients at 7- and 14 days post-transfer. The recipients were then infected intranasally with WSN-SIINFEKL to recall the persisting OT-1 cells expanded following DC immunisation. The kinetics of the expanded OT-I cells was analysed at different days post-infection (dpi). The animals were euthanized at 8 dpi for cellular analysis. ICCS assays were performed to assess the functionality of the activated OT-I cells by stimulating with SIINFEKL in the presence of Brefeldin A for four hours. The abundance of replicating virus particles in the lungs was measured by performing viral titration using MDCK cells or by qRT-PCR to measure the expression of genes for viral nucleoprotein (NP) and RNA-dependent RNA polymerase (RdRP).

Rab8a reconstitution in BM cells of aged mice and their functional characterisation

BM cells of aged (> 18 months) female mice were transduced with lentivirus harbouring the Rab8a construct by spin transduction[57].

The cells were then cultured in media supplemented with 5 ng/mL of GM-CSF and IL-4 for 5 days for differentiation of BMDCs. 5 days post culture, the BMDCs were harvested by gently scraping and DCs were sorted based upon CD11c staining. The cells were then pulsed with 200 µg/mL of Ova for 2 or 24 hours and washed twice with 1xPBS. The antigen-pulsed DCs were co-cultured with CFSE-labelled OT1 cells for 72 hours to measure T cell proliferation.

In another set of experiments, equal number of BMDCs from young (6-8 weeks), aged (>18 months), and Rab8a-Over Expressing cells of aged (>18 month) female mice were pulsed with Ova (200 µg/mL) for 2 hours, washed twice and transferred into young (6-8 weeks) $CD45.1^+$ female mice which were previously infused with CFSE labelled OT1 cells from young (6-8 weeks old) female mice. 72 hours post BMDCs transfer, peripheral blood was collected to analyse the expansion of the CFSE-labelled OT1 cells. The animals were left for one month and the persisting OT-I cells were recalled by intranasally (i.n) infecting the recipients with 200 pfu of WSN-SIINFEKL. The animals were euthanized and subjected to cellular analysis. Viral loads were measured by performing plaque assays. qRT-PCR was used for measuring the expression levels of genes for the viral NP and RdRP.

In an additional experiments, 3×10^4 of BMDCs differentiated from bone marrow cells of aged (>18 weeks) and young (6-8 weeks) female mice as well as those from aged (>18 months) mice following Rab8a over expression (Rab8a-OE) were pulsed with different concentrations of Ova or $Ova_{257\text{-}264}$ (SIINFEKL) peptide. The cells were then washed twice and co-cultured with 1.5×10^4 CFSE labelled OT1 cells for assessing the proliferation of OT1 cells from young (6-8 weeks old) female mice using flow cytometry.

In a separate experiment, young, aged and Rab8a-OE BMDCs generated according to the aforementioned protocols were pulsed with Ova (200 µg/mL) for 2 hours, washed twice with 1xPBS, and transferred into sex-matched $CD45.1^+$ female young (6-8 weeks) mice which were previously infused with CFSE labelled OT1 cells from sex matched young (6-8 weeks old) mice. 72 hours of DC therapy, different lymphoid organs were collected to analyse the expansion of CFSE-labelled OT1 cells. In the same experiment, the distribution of the BMDCs ($CD45.2^+CD11c^+$ Cells) within the organs was also assessed. The expression of chemokine receptors such as CCR5 and CCR7 was measured on IAV-pulsed BMDCs from each group. Additionally, Flt3l- DCs were generated from the bone marrow of young (6-8 weeks), aged (>18 weeks), and Rab8a-OE bone marrow cells of aged female mice. These cells were used to measure in vivo antigen presentation by transferring in $CD45.1^+$ young (6-8 weeks old) congenic female mice that had previously received OT1 cells from young (6-8 weeks old) mice. The experimental were performed as described above.

Measuring surface expression of SIINFEKL-H-$2K^b$ complexes on antigen-pulsed BMDCs

BMDCs were generated from female young (6-8 weeks), aged (>18 weeks old), and Rab8aOE conditions as described above. The cells were then pulsed with different concentrations of either complete Ova or $Ova_{257\text{-}274}$ (SIINFEKL) peptide for 6- and 24-hrs. The pulsed cells were then stained with antibodies against CD11c, class I MHC, and H-$2K^b$-SIINFEKL for 30 minutes at room temperature for detection of H-$2K^b$-SIINFEKL positive DCs out of class I MHC positive cells. The stained cells were washed twice with 1xPBS and then acquired using a BD Accuri C6 flow cytometer.

Assessing the in-vitro immune synapse formation using flow cytometry

BMDCs were generated from the bone marrow cells of young (6-8 weeks), aged (>18 months) and Rab8a reconstituted aged (>18 months old) by culturing them in media supplemented with 5 ng/mL of GM-CSF and IL-4 for 5 days for generation of BMDCs. The BMDCs were then sorted and labelled with celltrace™ Far Red and pulsed with either complete Ova or $Ova_{257\text{-}274}$ (SIINFEKL) peptide. The cells were then washed twice with 1xPBS and co-cultured with CFSE-labelled OT1 cells from sex matched young (6-8 weeks old) mice for 6hrs and 16hrs. The cells were then washed and acquired using a BD Accuri C6 flow cytometer.

Confocal microscopy

BM cells from female young (6-8 weeks) and aged (>18 months) animals were isolated and those from aged mice were then either transduced with lentiviruses packaged with Rab8a overexpressing constructs or vector controls. Following transduction, the young and aged cells were used to generate BMDCs by culturing them in the presence of GM-CSF and IL-4 as mentioned earlier. The frequency of $CD11c^+$ cells was assessed using flow cytometry and the cells were then seeded onto gelatine-coated coverslips overnight. The cells were pulsed with 200µg/mL of Ova for different time intervals (0hrs, 2hrs, 6hrs, 12hrs, and 24hrs). The cells were then washed twice with 1x PBS followed by fixing with 4% paraformaldehyde (PFA) for 20 minutes at room temperature. This was followed by blocking with 1% BSA in 1x PBS for 45 minutes. The cells were then washed and the Fc receptors were blocked using an Fc block reagent for 1 hour at room temperature. Fc blocking was followed by incubation with primary antibodies against Rab8a (mouse IgG) and Rab11 (rabbit IgG) for 2 hours. The primary antibody cocktail was prepared in an IC permeabilization solution procured from Invitrogen. The coverslips were then washed thrice with 1xPBS. This was followed by incubation with a cocktail of Hoechst, fluorescent-tagged secondary antibodies (anti-mouse IgG-Alexa Fluor 488 and anti-Rabbit IgG-Alexa Fluor 647) and anti-H-$2K^b$-SIINFEKL-PE prepared in IC permeabilization buffer for 2 hours. Following the incubation, the cells were washed thrice with 1xPBS and mounted on slides for image acquisition. The images were acquired using a Nikon A1 confocal microscope at 60x magnification. All the captured images were analysed by using ImageJ software. In the same experiment to visualise the total actin content inside the cells, CD11c positive cells generated from different conditions were fixed, permeabilized, and stained with Alexa Fluor™ 488 Phalloidin and acquired using BD Accuri C6 flow cytometer.

Fluorescence microscopy

Successful transfection of HEK293T cells for generation of Rab8a-shRNA and Rab8a-OE lentiviruses was confirmed using fluorescence microscopy after 72 hours of transfection. All the images were captured using a Leica microscope and analyzed using ImageJ software.

Cell lysate preparation and western blotting

Cell lysates were prepared using a hypotonic lysis buffer (20 mM HEPES, 0.2 mM EDTA, 1.5 mM $MgCl_2$, 100 mM KCl, 20 % (V/V) glycerol, 0.02% (V/V) NP-40, pH 7.5). The lysates were normalised using OD_{280} and resolved through SDS-PAGE (15% resolving, 4% stacking). The gels were transferred onto a PVDF membrane and blocked overnight at 4 °C using 5% skim milk in 0.05% PBST solution under slow rotation. On the next day, the membranes were washed thrice for 5 minutes each using 0.05% PBST solution and the blot was incubated with primary antibodies against Rab8a, Akt1, and pAkt1 (1:2000 dilution) for 1 hr at room temperature. GAPDH was used as an endogenous loading control. Following primary antibody incubation, the blot was washed 5 times with 0.05% PBST, and the blot was incubated with alkaline phosphatase-conjugated secondary antibodies for 45 minutes at room temperature. Following secondary antibody incubation, the blots were washed 5 times using 0.05% PBST and probed using femtolucent AP substrate solution. Additionally, cell lysate from ova pulsed BMDCs from young, aged, and Rab8a-OE were probed using primary anti-Rab8a and anti-Rab11 antibodies.

Plaque assay for virus titration

For measuring the viral load in the lungs of infected mice, the lungs were homogenised in serum-free DMEM using a tissue homogeniser. The homogenised samples were spun at 14000 g for 10 minutes at 4 °C and the supernatants were collected for viral titration on MDCK cells. After 5 days of infection, the plaques were developed by staining with crystal violet.

Statistical analysis

The exact P-values have been reported within the main figures itself. For comparison between two groups, a two-tailed paired t-test was used. For comparison between three groups, single factor ANOVA in the microsoft excel analysis toolpak (with $\alpha = 0.05$) was used, following which a Tukey-Kramer post hoc test was performed. The obtained q values were then checked for significance using a studentized q-table and were also used to generate the corresponding P-values using a self-written python script employing the scipy.stats module.

Reporting summary

Further information on research design is available in the Nature Portfolio Reporting Summary linked to this article.

Data availability

All data are included in the Supplementary Information or available with the authors, as are unique reagents used in this Article. The raw numbers for charts and graphs are available in the Source Data file whenever possible. The RNASeq data have been deposited in the Gene Expression Omnibus (GEO) repository under the accession number: GSE279003. Source data are provided with this paper.

References

1. Pennock, N. D. et al. T cell responses: naive to memory and everything in between. *Adv. Physiol. Educ.* **37**, 273–283 (2013).
2. Weyand, C. M. & Goronzy, J. J. Aging of the immune system. Mechanisms and therapeutic targets. *Ann. Am. Thorac. Soc.* **13**, S422–S428 (2016).
3. Nikolich-Žugich, J. The twilight of immunity: emerging concepts in aging of the immune system. *Nat. Immunol.* **19**, 10–19 (2018).
4. Ponnappan, S. & Ponnappan, U. Aging and immune function: molecular mechanisms to interventions. https://doi.org/10.1089/ars.2010.3228 (2011).
5. Crooke, S. N., Ovsyannikova, I. G., Poland, G. A. & Kennedy, R. B. Immunosenescence and human vaccine immune responses. *Immun. & ageing* **16**, 1–16 (2019).
6. Pinti, M. et al. Aging of the immune system: focus on inflammation and vaccination. *Eur. J. Immunol.* **46**, 2286–2301 (2016).
7. Lennon-Duménil, A. M. et al. Analysis of protease activity in live antigen-presenting cells shows regulation of the phagosomal proteolytic contents during dendritic cell activation. *J. Exp. Med.* **196**, 529–539 (2002).
8. Grant, E. P., Michalek, M. T., Goldberg, A. L. & Rock, K. L. Rate of antigen degradation by the ubiquitin-proteasome pathway influences MHC class I presentation. *J. Immunol. (Baltimore, Md. 1950)* **155**, 3750–3758 (1995).
9. Falo, L. D. Jr, Kovacsovics-Bankowski, M., Thompson, K. & Rock, K. L. Targeting antigen into the phagocytic pathway in vivo induces protective tumour immunity. *Nat. Med.* **1**, 649–653 (1995).
10. Kovacsovics-Bankowski, M. & Rock, K. L. A phagosome-to-cytosol pathway for exogenous antigens presented on MHC class I molecules. *Science.* **267**, 243–246 (1995).
11. Sato, T. et al. Rab8a and Rab8b are essential for several apical transport pathways but insufficient for ciliogenesis. *J. Cell Sci.* **127**, 422–431 (2014).
12. Nair-Gupta, P. et al. TLR signals induce phagosomal MHC-I delivery from the endosomal recycling compartment to allow cross-presentation. *Cell* **158**, 506–521 (2014).
13. Rosen, D. B. et al. Cutting edge: lectin-like transcript-1 is a ligand for the inhibitory human NKR-P1A receptor. *J. Immunol.* **175**, 7796–7799 (2005).
14. Bláha, J. et al. Structure of the human NK cell NKR-P1: LLT1 receptor: ligand complex reveals clustering in the immune synapse. *Nat. Commun.* **13**, 5022 (2022).
15. Palmieri, G. et al. CD94/NKG2-A inhibitory complex blocks CD16-triggered Syk and extracellular regulated kinase activation, leading to cytotoxic function of human NK cells. *J. Immunol.* **162**, 7181–7188 (1999).
16. Rodriguez-Barbosa, J. I. et al. HVEM, a cosignaling molecular switch, and its interactions with BTLA, CD160 and LIGHT. *Cell. & Mol. Immunol.* **16**, 679–682 (2019).
17. Filén, S. & Lahesmaa, R. GIMAP proteins in T-lymphocytes. *J. Signal Transduct.* **2010**, https://doi.org/10.1155/2010/268589 (2010).
18. Tolksdorf, F. et al. The PDL1-inducible GTPase Arl4d controls T effector function by limiting IL-2 production. *Sci. Rep.* **8**, 1–9 (2018).
19. McLellan, A. D. et al. Anatomic location and T-cell stimulatory functions of mouse dendritic cell subsets defined by CD4 and CD8 expression. *Blood. J. Am. Soc. Hematol.* **99**, 2084–2093 (2002).
20. Hong, W., Yang, B., He, Q., Wang, J. & Weng, Q. New insights of CCR7 signaling in dendritic cell migration and inflammatory diseases. *Front. Pharmacol.* **523**, https://doi.org/10.3389/fphar.2022.841687 (2022).
21. Nan, Y., Wu, C. & Zhang, Y.-J. Interplay between Janus kinase/signal transducer and activator of transcription signaling activated by type I interferons and viral antagonism. *Front. Immunol.* **8**, 1758 (2017).
22. Katze, M. G., He, Y. & Gale, M. Viruses and interferon: a fight for supremacy. *Nat. Rev. Immunol.* **2**, 675–687 (2002).
23. Marckmann, S. et al. Interferon-β up-regulates the expression of co-stimulatory molecules CD80, CD86 and CD40 on monocytes: significance for treatment of multiple sclerosis. *Clin. & Exp. Immunol.* **138**, 499–506 (2004).
24. Parlato, S. et al. Expression of CCR-7, MIP-3β, and Th-1 chemokines in type I IFN-induced monocyte-derived dendritic cells: importance for the rapid acquisition of potent migratory and functional activities. *Blood. J. Am. Soc. Hematol.* **98**, 3022–3029 (2001).
25. Channappanavar, R. & Perlman, S. Age-related susceptibility to coronavirus infections: role of impaired and dysregulated host immunity. *J. Clin. Invest.* **130**, 6204–6213 (2020).
26. Mueller, A. L., McNamara, M. S. & Sinclair, D. A. Why does COVID-19 disproportionately affect older people? *Aging (albany NY)* **12**, 9959 (2020).
27. Verity, R. et al. Estimates of the severity of coronavirus disease 2019: a model-based analysis. *Lancet Infect. Dis.* **20**, 669–677 (2020).
28. Yanez, N. D., Weiss, N. S., Romand, J.-A. & Treggiari, M. M. COVID-19 mortality risk for older men and women. *BMC Public Health* **20**, 1–7 (2020).
29. Singh, D. K. et al. Responses to acute infection with SARS-CoV-2 in the lungs of rhesus macaques, baboons and marmosets. *Nat. Microbiol.* **6**, 73–86 (2021).
30. Hadjadj, J. et al. Impaired type I interferon activity and inflammatory responses in severe COVID-19 patients. *Science.* **369**, 718–724 (2020).
31. Si, Y. et al. Lung cDC1 and cDC2 dendritic cells priming naive CD8+ T cells in situ prior to migration to draining lymph nodes. *Cell Rep.* **42**, https://doi.org/10.1016/j.celrep.2023.113299 (2023).
32. Joffre, O. P., Segura, E., Savina, A. & Amigorena, S. Cross-presentation by dendritic cells. *Nat. Rev. Immunol.* **12**, 557–569 (2012).

33. Sehrawat, S. et al. A catalytically inactive mutant of the deubiquitylase YOD-1 enhances antigen cross-presentation. *Blood. J. Am. Soc. Hematol.* **121**, 1145–1156 (2013).
34. Hickman, H. D. et al. CXCR3 chemokine receptor enables local CD8+ T cell migration for the destruction of virus-infected cells. *Immunity* **42**, 524–537 (2015).
35. van de Laar, L., Coffer, P. J. & Woltman, A. M. Regulation of dendritic cell development by GM-CSF: molecular control and implications for immune homeostasis and therapy. *Blood* **119**, 3383–3393 (2012).
36. Sukhbaatar, N., Hengstschläger, M. & Weichhart, T. mTOR-mediated regulation of dendritic cell differentiation and function. *Trends Immunol.* **37**, 778–789 (2016).
37. Wall, A. A. et al. Small GTPase Rab8a-recruited phosphatidylinositol 3-kinase γ regulates signaling and cytokine outputs from endosomal toll-like receptors. *J. Biol. Chem.* **292**, 4411–4422 (2017).
38. Kirkling, M. E. et al. Notch signaling facilitates in vitro generation of cross-presenting classical dendritic cells. *Cell Rep.* **23**, 3658–3672 (2018).
39. Chen, L. et al. Disruption of the AMPK-TBC1D1 nexus increases lipogenic gene expression and causes obesity in mice via promoting IGF1 secretion. *Proc. Natl. Acad. Sci. USA* **113**, 7219–7224 (2016).
40. Waskow, C. et al. The receptor tyrosine kinase Flt3 is required for dendritic cell development in peripheral lymphoid tissues. *Nat. Immunol.* **9**, 676–683 (2008).
41. Luo, L. et al. Rab8a interacts directly with PI3K$γ$ to modulate TLR4-driven PI3K and mTOR signalling. *Nat. Commun.* **5**, 4407 (2014).
42. Armstrong, J. et al. Identification of a novel member of the Rab8 family from the rat basophilic leukaemia cell line, RBL. 2H3. *J. Cell Sci.* **109**, 1265–1274 (1996).
43. Hattula, K. et al. Characterization of the Rab8-specific membrane traffic route linked to protrusion formation. *J. Cell Sci.* **119**, 4866–4877 (2006).
44. Rowe, R. K., Suszko, J. W. & Pekosz, A. Roles for the recycling endosome, Rab8, and Rab11 in hantavirus release from epithelial cells. *Virology* **382**, 239–249 (2008).
45. Grigoriev, I. et al. Rab6, Rab8, and MICAL3 cooperate in controlling docking and fusion of exocytotic carriers. *Curr. Biol.* **21**, 967–974 (2011).
46. Peränen, J. Rab8 GTPase as a regulator of cell shape. *Cytoskeleton* **68**, 527–539 (2011).
47. Pollard, T. D. & Cooper, J. A. Actin, a central player in cell shape and movement. *Science.* **326**, 1208–1212 (2009).
48. Peränen, J., Auvinen, P., Virta, H., Wepf, R. & Simons, K. Rab8 promotes polarized membrane transport through reorganization of actin and microtubules in fibroblasts. *J. Cell Biol.* **135**, 153–167 (1996).
49. Alraies, Z. et al. Cell shape sensing licenses dendritic cells for homeostatic migration to lymph nodes. *Nat. Immunol.* https://doi.org/10.1038/s41590-024-01856-3 (2024).
50. Gardner, I. D. The effect of aging on susceptibility to infection. *Rev. Infect. Dis.* **2**, 801–810 (1980).
51. Palucka, K. & Banchereau, J. Dendritic cells: a link between innate and adaptive immunity. *J. Clin. Immunol.* **19**, 12–25 (1999).
52. Kaur, M. et al. Galectin-3 regulates γ-herpesvirus specific CD8 T cell immunity. *IScience* **9**, 101–119 (2018).
53. Sehrawat, S. et al. CD8+ T cells from mice transnuclear for a TCR that recognizes a single H-2Kb-restricted MHV68 epitope derived from gB-ORF8 help control infection. *Cell Rep.* **1**, 461–471 (2012).
54. Singh, S. et al. Robust anti-SARS-CoV2 single domain antibodies cross neutralize multiple viruses. *IScience* **25**, 104549 (2022).
55. Sharma, Y. et al. A mouse model of PPRV infection for elucidating protective and pathological roles of immune cells. *Front. Immunol.* **12**, 1–19 (2021).
56. Livak, K. J. & Schmittgen, T. D. Analysis of relative gene expression data using real-time quantitative PCR and the 2-ΔΔCT method. *methods* **25**, 402–408 (2001).
57. Tehseen, A. et al. Glucocorticoid-mediated Suppression of Effector Programming Assists the Memory Transition of Virus-specific CD8+ T Cells. *J. Immunol*. https://doi.org/10.4049/jimmunol.2300513 (2024).

Acknowledgements

The authors would like to acknowledge the help provided by Nirmal Kumar and Tejal Pathak of Dr. Indranil Banerjee's lab at IISER, Mohali for some of the experiments. Sudhakar Singh received fellowship from Indian Council of Medical Research., Y.J.S., received fellowship from Council of Scientific & Industrial Research, and S.D., A.T., R.S., received their fellowships from Intramural funds from IISER Mohali. The study was supported by intramural funding from IISER Mohali and extramural grants from DST-IPA/2020/00091 and DST-IPA/2021/00136 to SS.

Author contributions

Conceptualisation: S. Sehrawat and S.S. Methodology: S.S., A.T., S.D., Y.J.S., R.S, S. Sehrawat. Writing- Original draft: S. Sehrawat and S.S.; Writing- Review and Editing: S.S., A.T. and S. Sehrawat. Visualisation & Data Presentation: S.S., A.T., and S. Sehrawat; Data curation & formal analysis: S.S., A.T., and S. Sehrawat; Supervision: S. Sehrawat; Funding acquisition: S. Sehrawat.

Competing interests

The authors declare no competing interests.

Additional information

Supplementary information The online version contains supplementary material available at https://doi.org/10.1038/s41467-024-54757-2.

Correspondence and requests for materials should be addressed to Sharvan Sehrawat.

Peer review information *Nature Communications* thanks the anonymous reviewer(s) for their contribution to the peer review of this work. A peer review file is available.